


Research Article

A speleothem record of seasonality and moisture transport around the 8.2 ka event in Central Europe (Vacska Cave, Hungary)

Attila Demény^{a,b,*} , György Czuppon^{a,b}, Zoltán Kern^{a,b}, István Gábor Hatvani^{a,b}, Dániel Topál^{a,b}, Máté Karlik^{a,b}, Gergely Surányi^c, Mihály Molnár^d, Gabriella Ilona Kiss^{d,e}, Máté Szabó^{a,b}, Chuan-Chou Shen^f, Hsun-Ming Hu^f and Zoltán May^g

^aInstitute for Geological and Geochemical Research, Research Centre for Astronomy and Earth Sciences, Budaörsi út 45, Budapest, H-1112 Hungary; ^bResearch Centre for Astronomy and Earth Sciences, MTA Centre of Excellence, Budapest, Konkoly Thege Miklós út 15–17., H-1121 Hungary; ^cWigner Research Centre for Physics, ELKH, Budapest, Konkoly-Thege Miklós út 29–33., H-1121 Hungary; ^dInstitute for Nuclear Research, ELKH, Debrecen, Bem square 18/c, H-4026 Hungary; ^eHigh-Precision Mass Spectrometry and Environment Change Laboratory (HISPEC), University of Debrecen, Doctoral School of Physics, 4032 Debrecen, Egyetem tér, 4032 Hungary; ^fDepartment of Geosciences, National Taiwan University, Taipei 10617, Taiwan, ROC and ^gInstitute of Materials and Environmental Chemistry, Research Centre for Natural Sciences, ELKH, Magyar tudósok körútja 2, Budapest, H-1117 Hungary

Abstract

A stalagmite was collected in northern Hungary from the Vacska Cave, where monitoring and ventilation-based site selection had been conducted. The stalagmite covers the 10–8 ka (relative to AD 1950) period, including the so-called 8.2 ka event, and showed preceding signs of climate change that were evaluated by petrographic observations, ¹⁴C activities, Sr concentrations, and stable isotope compositions of calcite and inclusion-hosted water. Comparisons of speleothem records show that isotope peaks at ca. 8.5 ka are related to a regional climate anomaly, rather than to a continental-scale event. In accordance with regional proxy records, the 8.2 ka event was associated with a series of temperature and precipitation amount changes, starting with cooling and a reduction in the winter-to-summer precipitation ratio, and then becoming a humid and warm phase at 8.15 ka. X-ray diffraction-based crystallinity parameter (FWHM) values provided evidence for diagenetic alteration of the stable oxygen isotope compositions of inclusion waters. Nevertheless, the stable hydrogen isotope compositions of inclusion waters and the oxygen isotope values of the host calcite revealed elevated d-excess values, and therefore increased Mediterranean moisture contribution during the 8.2 ka event, which indirectly indicate the southward displacement of moisture transport from the Atlantic Ocean.

Keywords: Speleothem, Stable isotope compositions, Fluid inclusions, Speleothem calcite crystallinity, Diagenesis, 8.2 ka event, Moisture transport, Hungary

(Received 21 December 2022; accepted 5 June 2023)

Introduction

The pioneering multiproxy analysis of the Greenland GISP2 ice core in Alley et al. (1997) detected a prominent climate anomaly between 8 ka and 8.4 ka (all ages in this paper are reported relative to AD 1950) and revealed its global significance. Ever since, the “8.2 ka event” has become common knowledge in paleoclimate research. Hundreds of studies have covered the appearance, magnitude, and duration of climate-proxy signals in various marine and terrestrial records, as well as conducted model calculations to analyze global and local temperature, precipitation, and seasonality changes associated with the 8.2 ka event. The 8.2 ka event is best observed in Greenland ice cores, where stable oxygen isotopic ($\delta^{18}\text{O}$) records show an approximately -2.5‰ peak (Thomas et al., 2007). The negative $\delta^{18}\text{O}$ change is generally attributed to the sudden cooling caused by low $\delta^{18}\text{O}$ freshwater discharge

from lakes Agassiz and Ojibway (in the area of the Laurentide ice-sheet) to the North Atlantic Ocean at 8.470 ka (Barber et al., 1999). The freshwater discharge not only changed the oxygen isotopic composition of the moisture source, but also disturbed the North Atlantic thermohaline circulation, resulting in a weakened Atlantic Meridional Overturning Circulation (AMOC) (Alley et al., 1997; Barber et al., 1999). Although this early freshwater discharge caused changes in North Atlantic Ocean current strengths (Tegzes et al., 2014), the AMOC was not severely affected, and only the 8.2 ka event *sensu stricto* was associated with significant AMOC reduction (e.g., Shi et al., 2020). The AMOC reduction, in turn, resulted in southward displacement of the Intertropical Convergence Zone (ITCZ) and increased the heat and moisture transport to the European continent, as reflected by speleothem stable isotope records (e.g., Sha et al., 2019; Demény et al., 2021a). The movement of the ITCZ dispersed the effects of the 8.2 ka climate change worldwide, producing a global signal (Cheng et al., 2009; Morill et al., 2013; Parker and Harrison, 2022). As such, the 8.2 ka $\delta^{18}\text{O}$ peak may be used as a time marker to verify age-depth models (Benson et al., 2021), and its analysis

*Corresponding author email address: demeny@geochem.hu

Cite this article: Demény A et al (2024). A speleothem record of seasonality and moisture transport around the 8.2 ka event in Central Europe (Vacska Cave, Hungary). *Quaternary Research* 118, 195–210. <https://doi.org/10.1017/qua.2023.33>



also can provide information on seasonal temperature and precipitation changes (Prasad *et al.*, 2009; Morill *et al.*, 2013; Peckover *et al.*, 2019). High-resolution analyses of several Greenland ice core $\delta^{18}\text{O}$ records led Thomas *et al.* (2007) to suggest a dual structure of the $\delta^{18}\text{O}$ peak, with a “whole event” from 8.247–8.086 ka and a “central event” from 8.212–8.141 ka. Brouard *et al.* (2021) reviewed 597 ^{14}C records from marine and continental archives and determined that a freshwater discharge occurred at 8.220 ka and a subsequent lake dam breakup occurred at 8.160 ka. These studies indicate that the 8.2 ka event potentially had a fine structure that may be associated with complex changes in precipitation,

as well as in temporal and spatial temperature variation (e.g., Seppä *et al.*, 2007; Prasad *et al.*, 2009).

Due to age uncertainties, it is sometimes difficult to determine if an individual $\delta^{18}\text{O}$ change in the paleoclimate record is related to the 8.2 ka event or if it represents a preceding or subsequent event, or even a broad period of climate change (Rohling and Pälike, 2005). Parker and Harrison (2022) provided a global compilation of well-dated speleothem records that were sampled at sufficient resolution (≤ 30 years). The global average start (8.223 ka) and end (8.062 ka) dates of the 8.2 ka $\delta^{18}\text{O}$ peaks (Fig. 1A) fit the ages reported by Thomas *et al.* (2007), suggesting

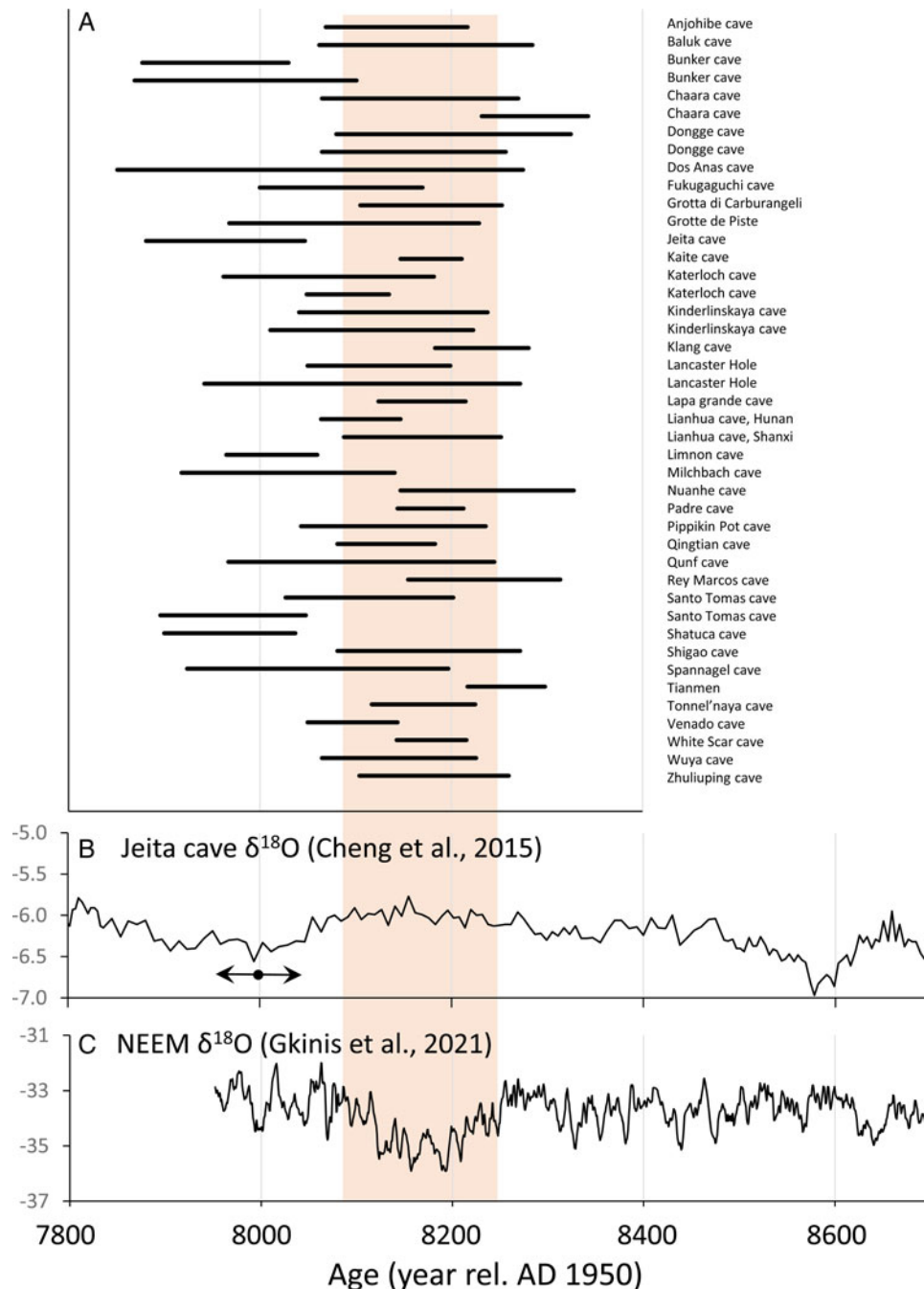


Figure 1. (A) List of $\delta^{18}\text{O}$ records compiled by Parker and Harrison (2022) in their Table S1, with the time intervals of their $\delta^{18}\text{O}$ peaks, as well as (B) the Jeita Cave (Cheng *et al.*, 2015) and (C) the NEEM ice core (Gkinis *et al.*, 2021) $\delta^{18}\text{O}$ records. The age uncertainty of the Jeita record is also shown with arrows. Shaded bar shows the interval of the “whole event” from 8.247–8.086 ka defined by Thomas *et al.* (2007). The $\delta^{18}\text{O}$ values are all in ‰ relative to VPDB (B) and VSMOW (C).

a globally coherent signal. However, some of the negative speleothem $\delta^{18}\text{O}$ peaks included in this calculation would fall outside the 8.2 ka period if the reported age uncertainties were considered. One of the most prominent records is the Jeita Cave (Lebanon) $\delta^{18}\text{O}$ record (Cheng et al., 2015; Fig. 1B), which is exceptionally well dated (63 age dates for the period of 12.180–1.210 ka and 5 ages for the 9–8 ka period, with an average age uncertainty of 42 years; Cheng et al., 2015). The Jeita $\delta^{18}\text{O}$ record is also exceptional because it contains strongly negative $\delta^{18}\text{O}$ shifts before and after the 8.2 ka event, which would indicate that the 8.2 ka peak of the Greenland ice core records (e.g., NEEM, Gkinis et al., 2021; Fig. 1C) would instead fit a positive shift in the Jeita record within the age uncertainties (Fig. 1). This observation raises the following questions: (1) is the 8.2 ka event represented exclusively by negative $\delta^{18}\text{O}$ shifts in Europe and the Mediterranean, and (2) are pre- and post-8.2 ka peaks also related to the multiple freshwater discharge events in the North Atlantic?

In this study, we present stable isotope and trace element records of a stalagmite from northern Hungary that covers the 10–8 ka period and indicates a climate change event at ca. 8.5 ka (Demény et al., 2022). Conventional high-resolution stable carbon and oxygen isotope analyses of stalagmite carbonate are supplemented with petrographic observations, stable hydrogen and oxygen isotope analyses of inclusion-hosted waters, X-ray

diffraction-based crystallinity measurements, Mg-P-Sr concentration determinations, and AMS ^{14}C analyses to determine temperature and precipitation changes during the 9–8 ka period, as well as to derive moisture transport information of the 8.2 ka event.

Cave site description

The Pilis Mountains consist primarily of Triassic limestones (Dachstein Limestone) and dolostones (Haas, 2001), but small outcrops of Oligocene Hárshegyi Sandstone are also found (Deák et al., 2007) in the vicinity of the Ariadne cave system. The Dachstein Limestone Formation is >1 km thick. The Vacska Cave (Fig. 2) is a part of the Ariadne cave system that contains seven caves, which are now interconnected due to cave exploration works. The Vacska Cave (47°41'N, 18°50'E) is 9298 m long and 206 m deep, with an entrance at 459 m asl.

The Ariadne cave system is in a densely forested area dominated by deciduous trees. Cave monitoring by temperature and CO_2 content, as well as drip-water pH, chemistry, and stable isotope compositions were conducted in 2019 and 2020 (Czuppon et al., 2022a, b). The local average annual surface air temperature between 2008 and 2020 was 10.4°C (measured directly above the cave) whereas the cave air temperature near the study site (Fennkőhāti chamber, Fig. 2) was $8.8 \pm 0.01^\circ\text{C}$ (Czuppon et al., 2022a). The mean annual precipitation amount between 1950

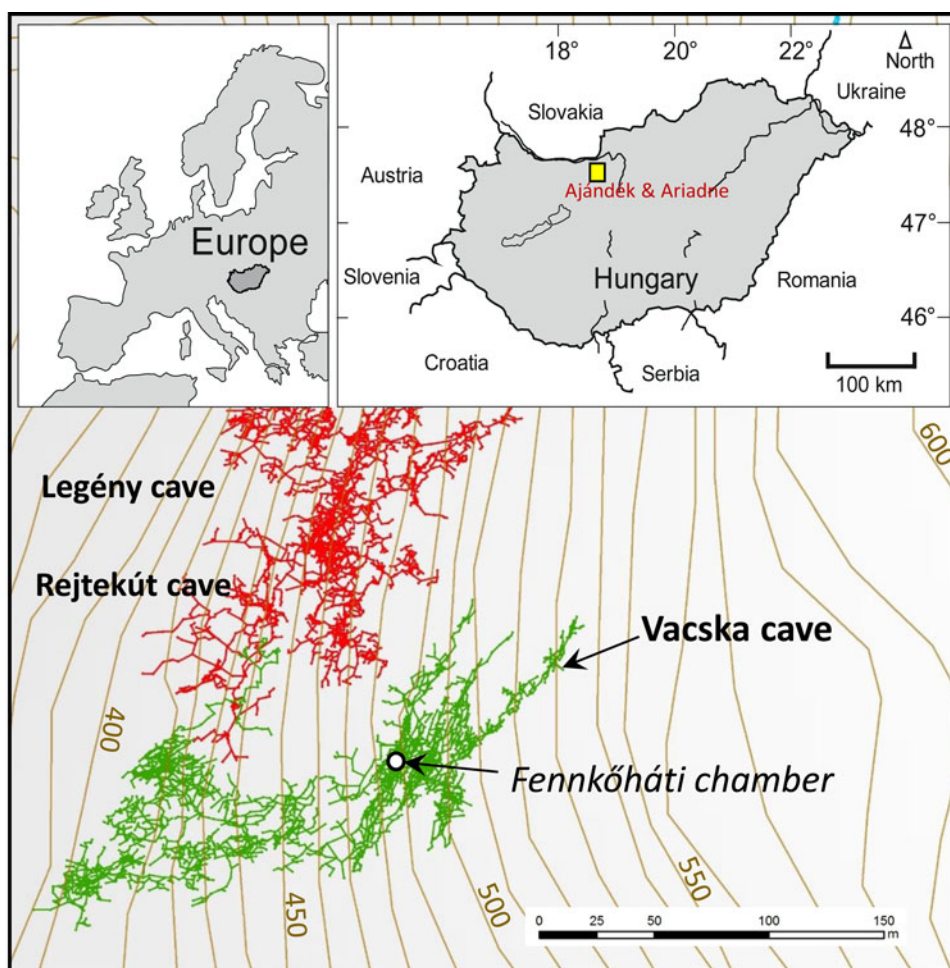


Figure 2. Location map of the Vacska Cave with the site (Fennkőhāti chamber) of the V-03 stalagmite.

and 2019 was 645 mm (min = 360 mm, max = 1200 mm). During this period, the most arid month was March (37 ± 24 mm), and the most humid month was June (76 ± 41 mm) (Supplementary Fig. 1).

The annual amount-weighted averages of the stable hydrogen and oxygen isotope compositions of precipitation at a nearby station (at Piliscsaba, ~8 km SE from the cave) were $\delta^2\text{H} = -60.1\text{‰}$ and $\delta^{18}\text{O} = -8.6\text{‰}$ in 2019 and 2020, respectively (Czuppon *et al.*, 2022a). The study site's drip water had slightly lower isotope compositions ($\delta^2\text{H} = -70.7 \pm 0.8\text{‰}$, $\delta^{18}\text{O} = -10.2 \pm 0.13\text{‰}$), indicating a 70–75% contribution of winter half-year precipitation to the drip water (Czuppon *et al.*, 2022a). The CO_2 concentration in the cave air varied between 550 ppmv (parts per million by volume) in winter and 9700 ppmv in summer during the 2019–2020 monitoring period (Czuppon *et al.*, 2022a). In general, the entire cave system is well ventilated. Czuppon *et al.* (2022b) searched for the least-ventilated part of the cave system using comprehensive stable isotope analysis of freshly precipitated carbonate on active speleothem surfaces. Although strongly positive C and O isotope correlations were found for many locations, indicating kinetic isotope fractionation due to ventilation, the deepest parts of Vacska Cave were found to be intact. As a result, a stalagmite (called V-03) that showed appropriate U and low Th concentrations (Czuppon *et al.*, 2022b) was selected from this sector for detailed analyses (Supplementary Fig. 2). These results are presented in this study.

Methods

Petrographic analysis and lamina counting were conducted on polished thin (~100 μm) sections using a Nikon Eclipse E600 POL optical microscope.

For the X-ray diffraction (XRD) analyses, 40 mg of finely powdered calcite samples were used in a suspension of 1 cm^3 ethanol and were dried on a $4 \times 3 \times 0.1$ cm metal sample holder. The XRD measurements were conducted using a Rigaku Miniflex600 powder diffractometer, with a 35 min analysis time, $2\text{--}70^\circ$ 2θ range, 0.05° step size, $2^\circ/\text{min}$ rate, Cu X-ray source, graphite monochromator, and scintillation counter. Full width at half maximum (FWHM) values were determined for the $2\theta = 29.39$ peak. The Philips X'pert Software (1.2a) was used for FWHM value calculations.

Sr concentrations were determined using a Spectro xSORT HH03 handheld energy-dispersive X-ray fluorescence (XRF) instrument, which consists of a Rh X-ray tube, two filters, and a silicon drift detector (SDD). Two spectra were recorded for optimum excitation of the X-ray tube values during measurements with 50 kV 0.05 mA and 15 kV 0.12 mA. The “FP- Mining” calibration developed by Spectro was used for the measurements. The instrument was slid along the surface of the stalactite in mm increments and provided information from a sample area of ~3 mm.

XRF analyses also were performed on stalagmites that previously had been measured by laser ablation inductively coupled mass spectrometry (LA ICP-MS). LA ICP-MS analyses were conducted on two stalagmites (Kiskóhát: Siklósy *et al.*, 2009; BAR-II L: Demény *et al.*, 2017) using a Perkin-Elmer ELAN 6100 DRC ICP-MS coupled with a LAMBDA PHYSICS excimer laser (193 nm) at the University of Lausanne (Siklósy *et al.*, 2009). The XRF-based and LA ICP-MS results are shown in Supplementary Figure 3. Although there are some sections where the two records do not match (BAR-II L: ~16–190 mm;

Kiskóhát: ~202–228 mm; Supplementary Fig. 3), most of the records are similar, and the major patterns are reproduced, supporting that XRF analyses can be used to detect major Sr concentration changes. The Sr concentration range of the V-03 stalagmite studied in this paper exceeds the XRF–ICP-MS difference, thus, the XRF-based Sr ppm variation may reflect primary, stalagmite-related features beyond analytical uncertainty.

Calcite samples were drilled from a polished stalagmite surface using a 0.6-mm drill bit. The entire stalagmite was sampled at a resolution of ~1 mm, but the section of 39.5–59.9 mm dft (distance from top) was sampled by drilling a trench with an average resolution of 0.1 mm (ranging from 0.04–0.2 mm, depending on the density of calcite laminations). Stable carbon and oxygen isotope compositions were determined using an automated carbonate preparation device (GASBENCH II) and a Thermo Finnigan delta plus XP continuous-flow mass spectrometer at the Institute for Geological and Geochemical Research, Research Centre for Astronomy and Earth Sciences (Budapest, Hungary). Three laboratory standards, calibrated using the NBS-18, NBS-19, and LSVEC reference materials (provided by the International Atomic Energy Agency), were used for sample standardization. These isotope compositions are expressed as $\delta^{13}\text{C}$ and $\delta^{18}\text{O}$ values (in ‰) relative to the Vienna Pee Dee Belemnite (VPDB). As a test of external precision, the Harding Iceland Spar (Landis, 1983) sample was measured as unknown and yielded $\delta^{13}\text{C}$ and $\delta^{18}\text{O}$ values of $-4.82 \pm 0.02\text{‰}$ and $-18.57 \pm 0.06\text{‰}$, respectively ($n = 57$ in the year of the V-03 analyses). These values agree with the published $\delta^{13}\text{C}$ and $\delta^{18}\text{O}$ values of -4.80‰ and -18.56‰ , respectively (Landis, 1983) (differences between the measured and published values indicate external accuracies).

Inclusion-hosted water was extracted by crushing speleothem chips in stainless steel tubes, followed by measurements of the stable hydrogen and oxygen isotope compositions with a model LWIA-24d (Los Gatos Research Ltd.) liquid water isotope analyzer, as described by Demény *et al.* (2016). The isotope compositions are expressed in conventional $\delta^2\text{H}$ and $\delta^{18}\text{O}$ values (as $\delta^{18}\text{O}_{\text{fi}}$ for fluid inclusions to distinguish from the calcite's $\delta^{18}\text{O}_{\text{cc}}$) relative to Vienna Standard Mean Ocean Water (VSMOW). Analytical accuracies are about $\pm 2\text{‰}$ for $\delta^2\text{H}$ and $\pm 0.5\text{‰}$ for $\delta^{18}\text{O}_{\text{fi}}$ on the basis of sample measurements with known isotopic compositions (Demény *et al.*, 2021b).

Twenty accelerator mass spectrometry (AMS) ^{14}C analyses were conducted for the entire stalagmite section. First, 10–20 mg of carbonate samples were treated with 85% orthophosphoric acid (H_3PO_4) in a vacuum-tight digestion reactor and kept overnight at 70°C to release the carbon as CO_2 . Next, the liberated CO_2 was purified and trapped cryogenically with a customized vacuum line (Molnár *et al.*, 2013a). AMS graphite targets were prepared from the CO_2 samples by a customized sealed tube graphitization method (Rinyu *et al.*, 2013). The $^{14}\text{C}/^{12}\text{C}$ ratios were determined at the EnvironMICADAS ^{14}C facility (Molnár *et al.*, 2013b), Hertelendi Laboratory of Environmental Studies at the Institute for Nuclear Research, (Debrecen, Hungary).

Uranium series dating analyses were performed on 14 samples at the Isotope Climatology and Environmental Research Centre at the Institute for Nuclear Research (Debrecen, Hungary). The analyzed parts of the samples were completely dissolved in diluted (~10%) hydrochloric acid (HCl). The samples were then spiked with a $^{229}\text{Th}/^{233,236}\text{U}$ tracer to remove organic material, after which they were converted to nitric form by boiling nitric acid

(HNO₃). The U/Th separations were conducted with extraction chromatography on UTEVA resin. The final fractions were measured using a Thermo Scientific Neptune Plus MC-ICPMS. The uncertainties of the ages were calculated with the Monte Carlo method.

The calcite samples used earlier for fluid inclusion analyses were powdered, and batches were selected for trace element analyses to ensure there was sufficient material. The powdered samples were divided into two parts for two parallel measurements. The samples (~100–300 mg) were weighed with an analytical scale into glass beakers to which 3 ml of concentrated HCl (37%, Suprapur grade) was slowly added. After 30 minutes, the solution was transferred into a volumetric flask and topped up to 20 ml with ultrapure water (SUEZ, 18.2 MΩ/cm). The trace element concentrations of the sample solutions were measured with a Spectro Genesis Inductively Coupled Plasma Optical Emission Spectroscopy (ICP-OES) simultaneous spectrometer, with axial plasma observation system. The instrument was calibrated with a multielement standard (LobaChemie, Multielement Standard Solution for ICP 33 components 100 mg/l).

The studied stalagmite

The V-03 stalagmite was collected near the Fennkőháti chamber (Fig. 2). The stalagmite formed on a flowstone layer that was later broken either by rock movements or during cave exploration. It is 15.2 cm from the flowstone base, with a diameter of ~7.5 cm (Supplementary Fig. 2). The stalagmite is composed of finely laminated clear calcite with no visible hiatus. The laminae have flat tops that are ~3 cm wide. No pores are visible in the axial part, although some pores appear at the flanks. The lamination is expressed by thin, brownish layers, which likely contain organic material, and the alternation of inclusion-poor and inclusion-rich layers (Fig. 3). The stalagmite's fabric is dominated by columnar calcite with a varying elongation rate (Supplementary Fig. 2).

The present study focuses on the part that is 45–85 mm from the top of the stalagmite and is covered by one thin section. This section is dominated by elongated, compact columnar calcite (Fig. 3). From ~81 mm to ~78 mm dft (distance from top), the growth direction is shifted, and then growth continues in the original direction. This shift is expressed by the calcite crystals, as well as the fluid inclusion distribution (Fig. 3). Large inclusions, representing inter-crystalline voids, appear in several layers at 73 mm, 67 mm, and 52 mm dft. At 48.0 mm dft, there is a hiatus with flat crystal terminations, followed by new crystal formation. The surface of the hiatus is sharp, possibly suggesting erosion, but the “mesa” and “valley” forms (Railsback et al., 2013), which would indicate strong erosion, are absent. The surface is composed of pure and clean calcite, lacking the detrital material that would have been deposited if the surface underwent prolonged dry exposure. Thus, the hiatus is considered to be a short-term growth stop with dissolution.

Results

Fourteen U-Th age determinations were conducted on the section 15–145 mm dft (Supplementary Table 1). Excluding one outlier (at 55 mm dft; Supplementary Fig. 2), the age-depth relationship was established using the StalAge algorithm (Scholz and Hoffmann, 2011) (Supplementary Fig. 2). The ages range between $10,220 \pm 165$ years at 141 mm dft and 8140 ± 130 years at 16 mm dft. The 2σ uncertainties range from 125–270 years, with an average of 166 years. Although the StalAge algorithm cannot handle

the hiatus detected at 48.0 mm dft, the distribution of ages indicates that the hiatus did not span more than some decades, and thus was not investigated further.

To determine the recent contribution of rock-related carbon (“dead carbon proportion” [dcp]) at the study site, the top layer of a recently forming stalagmite (V-01) collected in the Vacska Cave, representing the 2008–2020 period (Demény et al., 2021c), also was analyzed (Supplementary Table 2). The average atmospheric CO₂ radiocarbon activity value, which was calculated from the datasets of Hua et al. (2013) and Major et al. (2018), yielded a percentage modern carbon (pMC) value of 102.09. This value, together with the measured pMC value of the V-01 stalagmite (97.19; Table 1), yields a dcp value of 4.8%. The V-03 ¹⁴C data increase from 29.93 ± 0.12 pMC to 37.89 ± 0.14 pMC without a major jump (Supplementary Table 2). The V-03 ¹⁴C ages were corrected for a set of potential dcp values from 4–10%. The dcp-corrected ¹⁴C ages were calibrated using OxCal 4.1 (Bronk Ramsey, 2001) and the IntCal20 dataset (Reimer et al., 2020). Age-depth relationships were modeled using the P_Sequence function (Bronk Ramsey, 2008). The best visual match of the U-Th ages and the StalAge age-depth relationship was observed with the AMS ¹⁴C deposition chronologies considering dcp corrections from 5–8% and (Fig. 4). This dcp range is usual among similar karstic environments in the region (Molnár et al., 2006, 2016; Demény et al., 2019b). Most of the U-Th ages plot within the 5% and 8% dcp age-depth models (Fig. 4), except the 40–70 mm dft section, in which elevated dead carbon contribution can be assumed.

The younger part of the stalagmite (~7 cm dft) showed clearly visible lamination under the binocular and optical microscopes. As such, this section was used for lamina counting, under the assumption that a single lamina would represent an annual layer. Laminae were counted starting at 71.0 mm dft at a U-Th dating spot that yielded 8450 ± 160 (2σ) years. Within the topmost 71-mm lamina, counts were conducted in 8 subsections, and the lamina numbers were subtracted. The lamina-based age model, starting from 8450 years (Fig. 4) closely follows both the StalAge-based and the ¹⁴C-based age-depth relationships that support the use of the StalAge model ages. However, lamina counting was not used to improve the U-Th age-based StalAge model, because detection of annual laminae is not definitively proven.

The XRF-based Sr concentrations and stable C-O isotope compositions of the stalagmite calcite (Supplementary Table 3) are shown in Figure 5, along with the U-Th ages and the StalAge age-depth model curve. Compared to the 0–100 mm section, the $\delta^{13}\text{C}$ record shows strong fluctuation below 100 mm dft, with several positive shifts (between ~140–150 mm, at ~123 mm, and at ~100–106 mm), and a negative peak at 116 mm dft. The $\delta^{18}\text{O}_{\text{cc}}$ record shows smaller variations in the 0–40 mm and 90–140 mm dft sections, whereas the 40–90 mm dft section is characterized by stronger $\delta^{18}\text{O}_{\text{cc}}$ fluctuation. The lowermost $\delta^{18}\text{O}_{\text{cc}}$ value in this section is at 52.17 mm dft (8190 ± 105 years), so the peak is tentatively attributed to the 8.2 ka peak (Fig. 5). A similar shift is visible at 82.7 mm dft (corresponding to a StalAge model age of 8524 years). The Sr concentration scatters between 32 ppm and 46 ppm.

A short-term hiatus is indicated by a break in the records at 48 mm (Fig. 5). Just before the hiatus, the $\delta^{13}\text{C}$ values strongly fluctuate and the Sr concentrations are low. Directly after the hiatus, the $\delta^{13}\text{C}$ values decrease and the Sr concentrations are higher than they were before the hiatus.

The calcite and fluid-inclusion isotope compositions (Supplementary Table 4) are plotted as a function of age in Figure 6. High-resolution drilling was conducted in the 8.105–

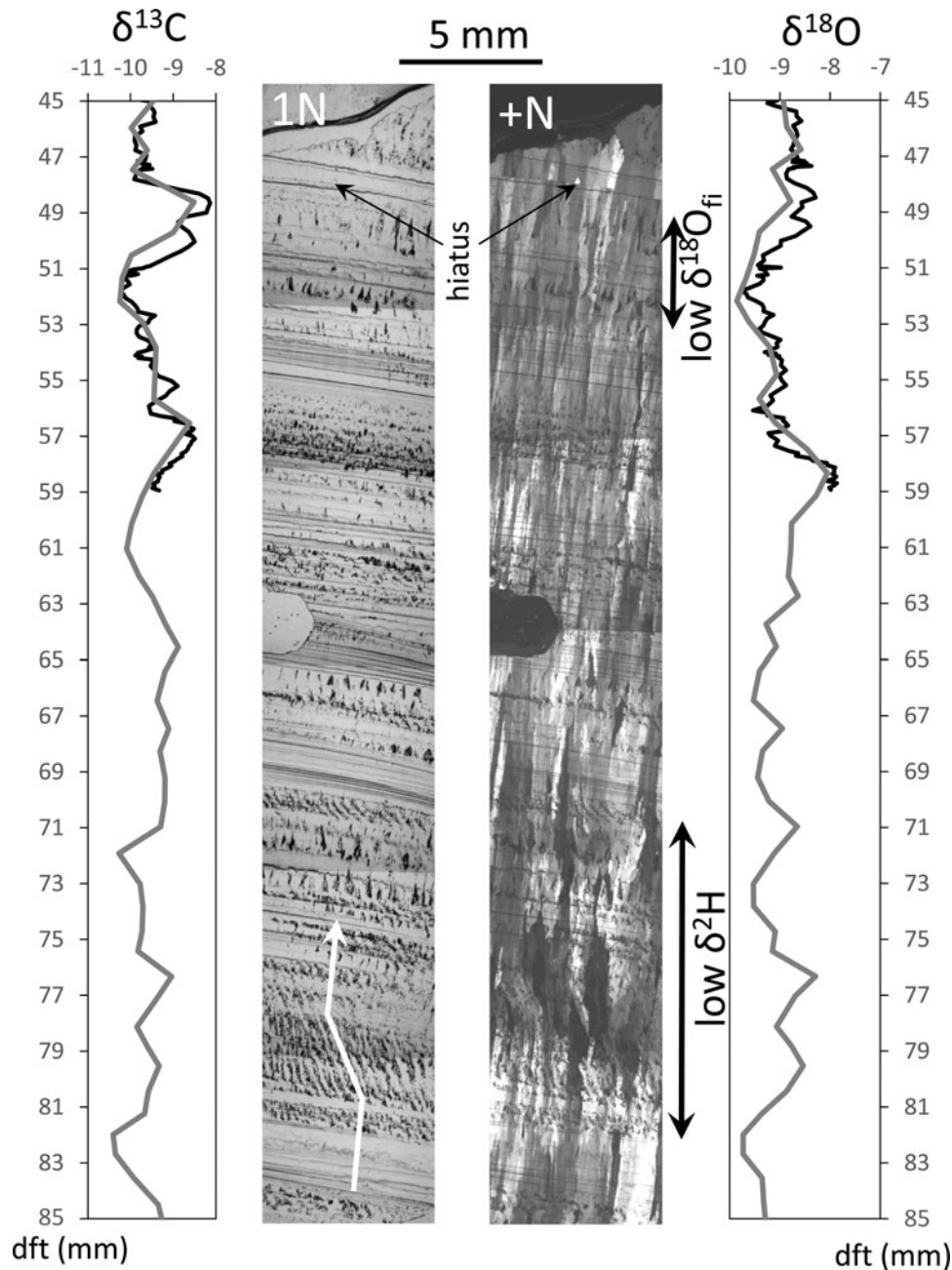


Figure 3. Optical microscope images of the 45–85 mm dft (distance from the top, in mm) interval with one nicol (1N) and crossed nicols (+N), as well as the stable C and O isotope compositions (in ‰ relative to VPDB). White arrow shows a fabric change where fluid inclusion trails are shifted, indicating drifting growth axis. Subsections with low hydrogen and oxygen isotope compositions of inclusion water are also shown. The hiatus at 48.0 mm dft is marked by arrows. $\delta^{13}\text{C}$ and $\delta^{18}\text{O}$ records: gray lines = low-resolution sampling; black lines = high-resolution sampling.

8.252 ka (39.5–59.9 mm dft) section to determine if additional peaks were detectable at a resolution of ~ 0.1 mm (ca. 1 year). The high resolution $\delta^{13}\text{C}$ – $\delta^{18}\text{O}$ records reproduced the low-resolution records without significant deviations (Figs. 3, 6). The patterns of stable H and O isotope compositions of inclusion-hosted water ($\delta^2\text{H}$, $\delta^{18}\text{O}_{\text{fi}}$) are different from those of the calcite records (Fig. 6). The $\delta^{18}\text{O}_{\text{fi}}$ values fluctuate between -12.8% and -8.6% , and one sampling section yielded a very low $\delta^{18}\text{O}_{\text{fi}}$ value (-15.8%) at 8.196 ka. This sample overlaps with the C–O isotope sampling section containing the lowest $\delta^{18}\text{O}_{\text{cc}}$ value. The $\delta^2\text{H}$ values range from -83.1% to -66.6% and are not correlated with the other isotope records. The lowermost $\delta^2\text{H}$ values

were obtained for the section of 8.521–8.433 ka. The 8.2 ka event's period is not associated with an appreciable $\delta^2\text{H}$ shift; only a slight indication of a negative $\delta^2\text{H}$ shift appears compared to the preceding and subsequent samples.

FWHM values were determined for the $2\theta = 29.4^\circ$ calcite XRD peak and are listed in Supplementary Table 4. The FWHM values are positively correlated with the $\delta^{18}\text{O}_{\text{fi}}$ values ($r = 0.62$, $p = 0.02$; Fig. 7; excluding the sample with $\delta^{18}\text{O}_{\text{fi}}$ value = -15.8% would not change the correlation parameters) and show no relationship with the $\delta^2\text{H}$ data ($r = -0.08$, $p = 0.78$).

The ICP-MS-based trace element concentrations and stable isotope compositions of subsamples crushed for fluid inclusion

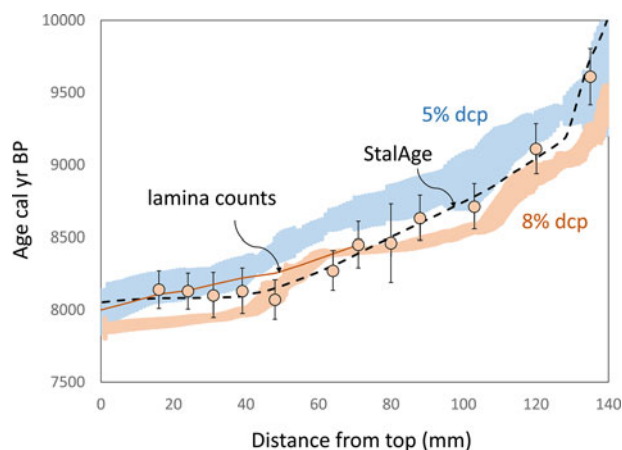


Figure 4. U-Th ages (with 2σ uncertainties), and AMS ^{14}C -based age models assuming 5% (blue shading) and 8% (brown shading) dead carbon proportion (dcp), the StalAge-based age-depth model (dashed line), and lamina-counting results (solid line) for the V-03 stalagmite. See text for details.

analyses are listed in Supplementary Table 5. Because these materials were subsamples of other analyses, they are not compared with other, distance-controlled data. However, their internal relationships were investigated. The Mg contents range from ~ 900 ppm to ~ 1200 ppm, the P contents from 27–69 ppm, and the Sr concentrations from 23–29 ppm. The correlations are also given in Supplementary Table 5. The most significant correlation is between the $\delta^{13}\text{C}$ values and P concentrations, with $r = -0.82$ and $p = 0.00$.

Discussion

General interpretations of chemical and isotopic proxies

This study utilizes Sr and P concentrations, stable carbon and oxygen isotope compositions of calcite, and stable hydrogen and oxygen isotope compositions of inclusion-hosted water, the basic interpretations of which are briefly summarized here.

The Sr content of speleothem calcite is determined by the Sr content of drip water, the partition coefficient between carbonate and water, and the carbonate precipitation rate (Huang and Fairchild, 2001). The Sr content of drip water is governed by rock weathering in the soil zone, the degree of carbonate rock dissolution, prior calcite precipitation (PCP) along the water migration route, and dilution due to increased precipitation and water seepage (Sinclair, 2011; Fairchild and Baker, 2012; Borsato et al., 2016). PCP is associated with a coupled increase in the $\delta^{13}\text{C}$ and $\delta^{18}\text{O}$ values of the precipitating carbonate (Fairchild and Baker, 2012; Steponaitis et al., 2015; Dreybrodt and Fohlmeister, 2022), so the presence of a positive Sr– $\delta^{13}\text{C}$ – $\delta^{18}\text{O}$ correlation may indicate PCP, whereas the absence of a positive $\delta^{13}\text{C}$ – $\delta^{18}\text{O}$ correlation may suggest the opposite. Because neither a significant change in growth rate nor a positive $\delta^{13}\text{C}$ – $\delta^{18}\text{O}$ correlation is observed in the V-03 stalagmite, the Sr content variation may be related to hydrological conditions such as precipitation amount (dilution effect) and changes in water residence time.

The stable carbon isotope composition of speleothem carbonate is affected by various factors, such as vegetation type, biogenic activity in the soil zone, carbonate rock dissolution, PCP, and kinetic fractionations during speleothem deposition

(see Fairchild and Baker, 2012, and references therein). In the absence of coupled $\delta^{13}\text{C}$, $\delta^{18}\text{O}$ and Sr content changes, PCP and ventilation-driven kinetic fractionation (Mickler et al., 2006; Steponaitis et al., 2015) can be excluded. Due to the short time period covered by the studied stalagmite, significant changes in vegetation type (^{13}C -enriched C_4 or ^{12}C -enriched C_3 plants) also can be dismissed. Biogenic activity in the soil manifests in the amount of ^{12}C in the dissolved CO_2 and, therefore, in the precipitating carbonate. Biogenic activity increases under humid conditions, so the $\delta^{13}\text{C}$ values may indicate variations in the amount of precipitation. Additionally, organic ligands in the drip water may transport phosphorus, which is adsorbed on the surface of the precipitating carbonate (Fairchild et al., 2001). Negative $\delta^{13}\text{C}$ –P relationships (i.e., less biogenic ^{12}C in the DIC, higher $\delta^{13}\text{C}$ in the speleothem carbonate, and less phosphorus transported by the drip water) have been found in speleothems from southern (Demény et al., 2019a) and northern (Demény et al., 2019b) Hungary, suggesting that a negative $\delta^{13}\text{C}$ –P relationship may indicate paleohydrological control. Batches of carbonate samples used for analyses of inclusion water contents also were selected to determine P, Mg, and Sr concentrations (Supplementary Table S5). The $\delta^{13}\text{C}$ values of the sample batches have no relation to the Mg contents, but they show a weak positive correlation with the Sr concentrations and a negative correlation with the P concentrations. This is in accordance with the assumption that humid conditions with elevated precipitation amounts result in drip water dilution (lower Sr content) and improved soil activity (lower $\delta^{13}\text{C}$, higher P), which were also observed in two other Hungarian caves (Demény et al., 2019a, b).

The oxygen isotope composition of speleothem calcite is determined by the drip water composition, formation temperature, and the temperature dependence of calcite–water oxygen isotope fractionation (McCrea, 1950, as the first study; Johnston et al., 2013, for empirical speleothem data). Additionally, site-related fractionation processes, such as ventilation-driven degassing and evaporation, or PCP may cause kinetic fractionation, affecting the $\delta^{13}\text{C}$ and $\delta^{18}\text{O}$ values of speleothem calcite. However, the kinetic fractionations may result in positive $\delta^{13}\text{C}$ – $\delta^{18}\text{O}$ correlations (Mickler et al., 2004, 2006). Positive $\delta^{13}\text{C}$ – $\delta^{18}\text{O}$ correlations also may be caused by climatic factors. For example, a warm and dry period may result in elevated $\delta^{13}\text{C}$ values due to a decrease in biogenic activity, and higher $\delta^{18}\text{O}$ values in the drip water. The drip water oxygen isotope composition also may be affected by several factors, including changes in vapor source composition, moisture transport trajectory, seasonality (winter/summer precipitation ratio), air temperature, and precipitation amount (e.g., Lachniet, 2009). Kern et al. (2019) compiled speleothem and precipitation composition data, as well as determined the effects of regional temperature variation and precipitation amount. The $\delta^{18}\text{O}$ value of local precipitation depends primarily on the precipitation amount in the Mediterranean, whereas the Carpathian Basin is characterized by temperature-dependence of the $\delta^{18}\text{O}_{\text{water}}$ values. The $\delta^{18}\text{O}$ –temperature relationship is usually higher ($\sim 0.6\text{‰}/^\circ\text{C}$, Kern et al., 2019; Demény et al., 2021b) than that of calcite–water oxygen isotope fractionation ($-0.23\text{‰}/^\circ\text{C}$; Tremaine et al., 2011). As such, the $\delta^{18}\text{O}_{\text{cc}}$ value is mainly governed by surface-air temperature changes, provided that the calcite is formed under equilibrium conditions. Under arid conditions, however, the precipitation water may experience evaporation and ^{18}O -enrichment that may be transferred to the speleothem site. This is why the $\delta^{18}\text{O}$ values should be interpreted in combination with other proxy data.

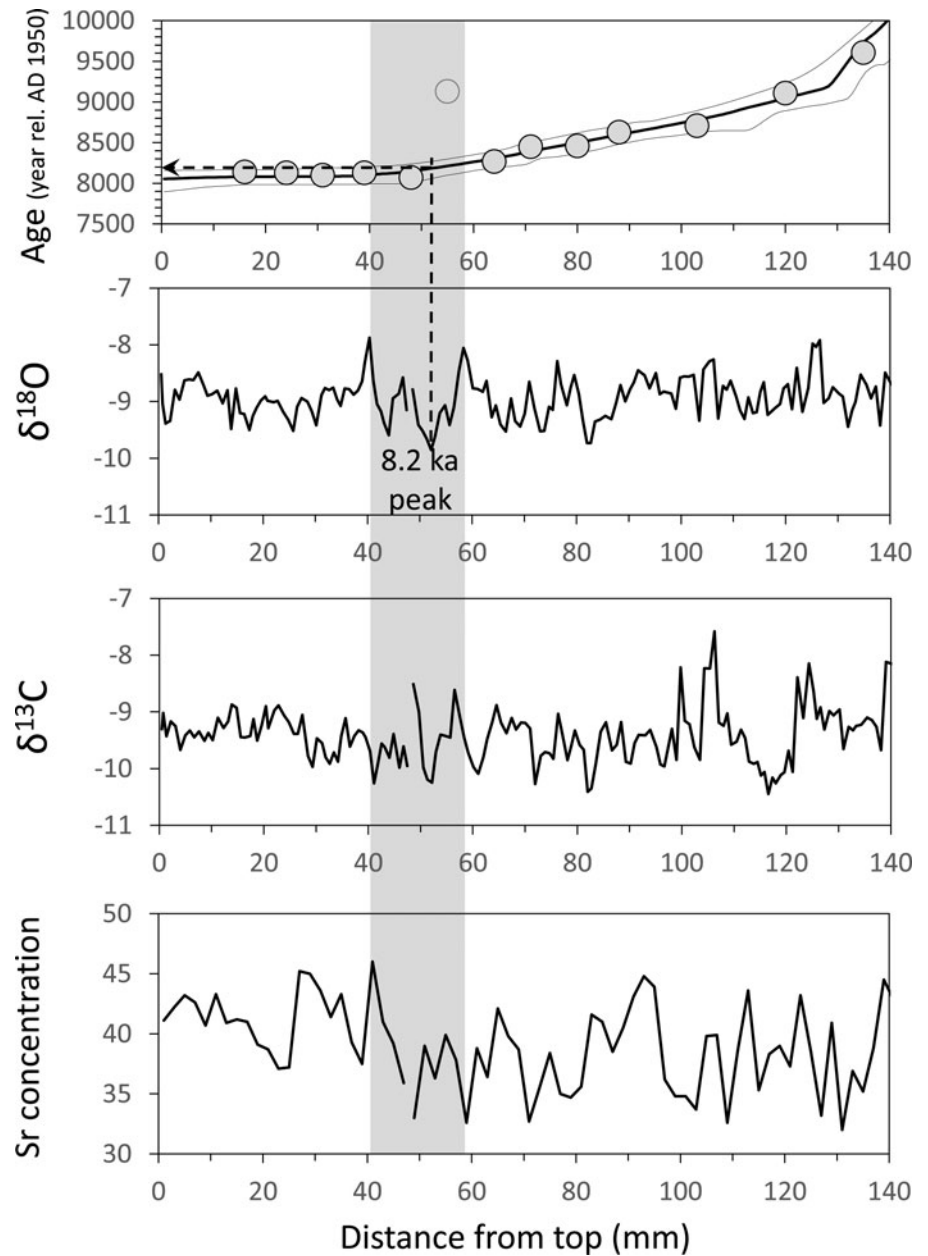


Figure 5. Sr concentration (in ppm), with stable carbon and oxygen isotope compositions of stalagmite calcite (in ‰ relative to VPDB), U-Th ages, and the StalAge-based age-depth model (with 2σ uncertainty ranges). The shaded bar marks the low- $\delta^{18}\text{O}$ peak tentatively related to the 8.2 ka event.

In theory, the stable hydrogen and oxygen isotope values of fluid inclusion-hosted water should directly reflect drip water compositions, provided that late-stage alterations have not modified the original compositions.

Diagenetic alterations versus primary signals

In general, the $\delta^2\text{H}$ values are regarded as intact regarding diagenesis due to the lack of hydrogen in the host calcite. However, because both the host calcite and the inclusion-hosted H_2O contain oxygen, diagenetic alteration may change the original $\delta^{18}\text{O}_{\text{fi}}$ value (Demény et al., 2016), leading to independent $\delta^2\text{H}$ and $\delta^{18}\text{O}_{\text{fi}}$ patterns. As detected by earlier analyses, calcite recrystallization is reflected by FWHM values (Demény et al., 2016). The width of the $2\Theta = 29.39$ XRD peak is determined by the calcite-crystal domain size and lattice strain, but significant lattice deformation is not expected in the case of speleothems, consequently

the FWHM changes may indicate crystal size variation (Demény et al., 2016). Furthermore, the sizes of calcite crystallites within the speleothem are determined by the original domain size of the carbonate precipitate and subsequent crystallization processes.

To investigate if diagenetic alteration may have influenced the $\delta^{18}\text{O}_{\text{fi}}$ values, crystallinity measurements were conducted on the same samples that underwent fluid inclusion analyses. The FWHM values are positively correlated with the $\delta^{18}\text{O}_{\text{fi}}$ data. However, to quantify the $\delta^{18}\text{O}_{\text{fi}}$ shifts during re-crystallization and to make the changes comparable to other occurrences, the differences between the inclusion-hosted water oxygen isotope compositions and the local drip water $\delta^{18}\text{O}$ value (-11.2‰ ; Czuppon et al., 2022a) were plotted as a function of FWHM values (Fig. 7). The data of Demény et al. (2016), which were gathered for a flowstone deposit of the Béke Cave (northeastern Hungary), are also shown in Figure 7. The slope of the V-03

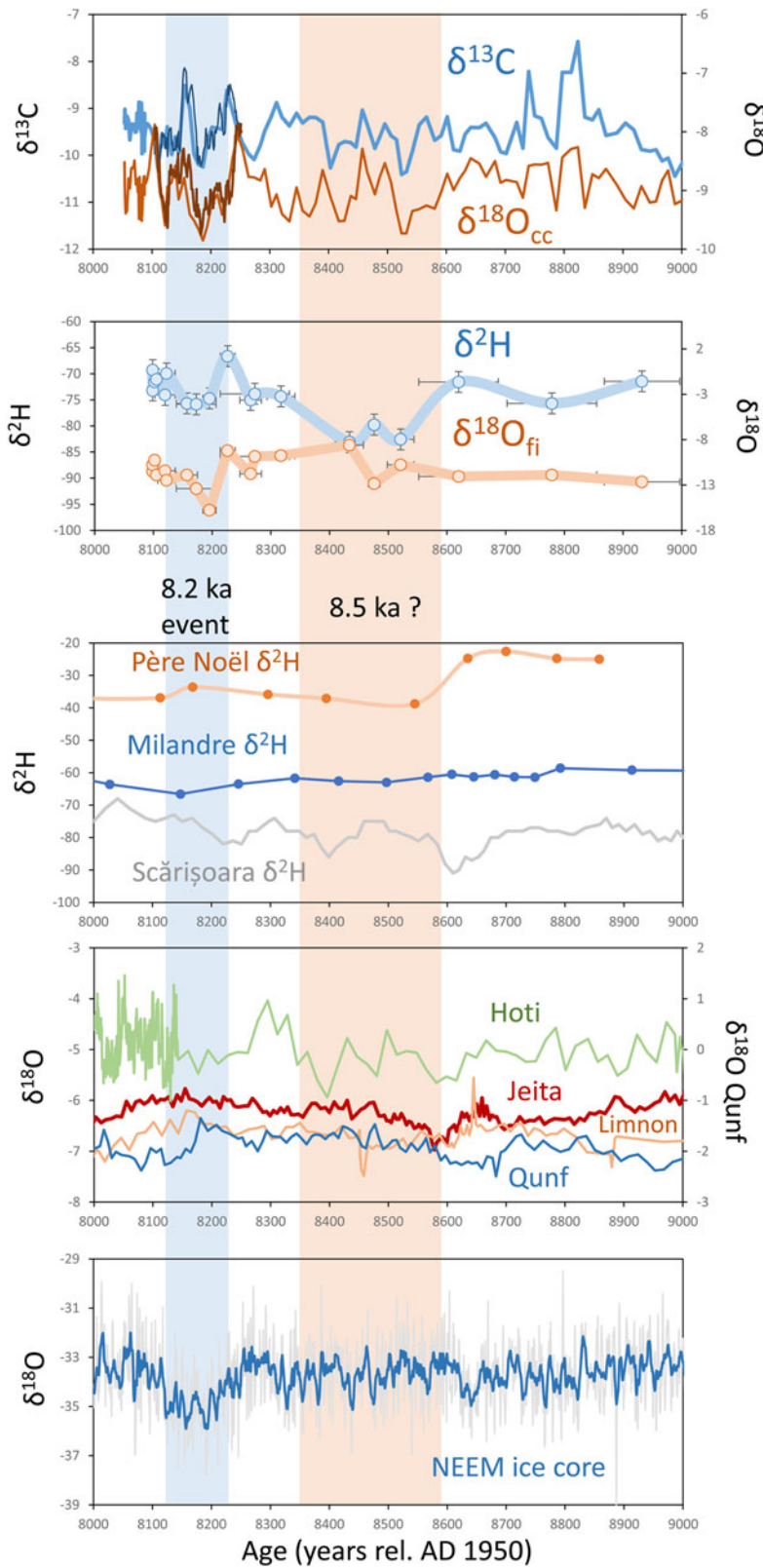


Figure 6. Stable hydrogen, with carbon and oxygen isotope compositions of the V-03 stalagmite calcite ($\delta^{13}\text{C}$ and $\delta^{18}\text{O}_{\text{cc}}$, in ‰, relative to VPDB) and inclusion-hosted water ($\delta^2\text{H}$ and $\delta^{18}\text{O}_{\text{fi}}$, in ‰, relative to VSMOW) and published records. Inclusion-hosted water compositions (in ‰, relative to VSMOW) for the Père Noël Cave (Belgium) from Allan et al. (2018); inclusion-hosted water compositions for the Milandre Cave (Switzerland) from Affolter et al. (2019); cave ice data from the Scărișoara Cave from Perșoiu et al. (2017). Calcite $\delta^{18}\text{O}$ records (in ‰ relative to VPDB) from the Limnon, Hoti, Qunf, and Jeita caves are from Peckover et al. (2019), Neff et al. (2001), Fleitmann et al., 2007, and Cheng et al. (2015), respectively. The $\delta^{18}\text{O}$ record of the NEEM ice core (blue line = 10-year moving average) is from Gkinis et al. (2021).

data is very similar to the slope found for the Béke Cave flowstone (Demény et al., 2016), indicating a general diagenetic process.

The diagenetic alteration detected by FWHM analysis raises the question of whether the $\delta^{18}\text{O}_{\text{cc}}$ data also were affected,

which may bias the $\delta^{18}\text{O}_{\text{cc}}$ -based temperature calculations. Assuming that the $\delta^{18}\text{O}_{\text{cc}}$ values are primary compositions related to equilibrium calcite-water oxygen isotope fractionation and that the $\delta^2\text{H}$ values reflect the composition of the drip water from

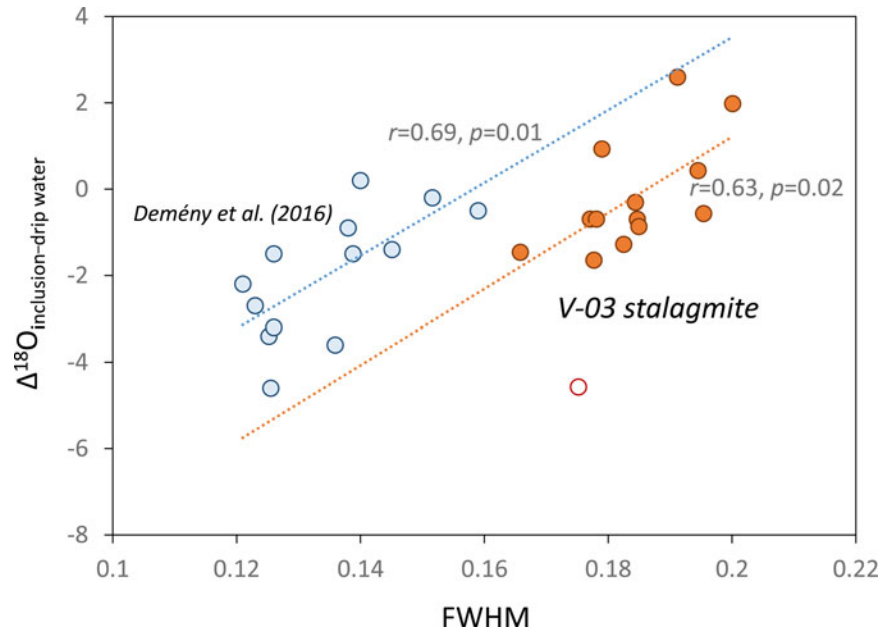


Figure 7. $\delta^{18}\text{O}$ deviations (in ‰; $\Delta^{18}\text{O}_{\text{inclusion-drip water}} = \delta^{18}\text{O}_{\text{in}} - \delta^{18}\text{O}_{\text{drip water}}$) of inclusion-hosted water compositions from local drip-water $\delta^{18}\text{O}$ values as a function of full width at half maximum (FWHM) values.

which the calcite precipitated, combining these data would yield reliable formation temperatures. Using a local meteoric-water line equation, the water $\delta^{18}\text{O}$ values ($\delta^{18}\text{O}_{\text{w}}$) can be estimated from the $\delta^2\text{H}$ data, while the formation temperature is given by the $\delta^{18}\text{O}_{\text{cc}} - \delta^{18}\text{O}_{\text{w}}$ fractionation and the relevant fractionation equation (Demény et al., 2021b). The fractionation equation of Johnston et al. (2013) was applied in this study because it also contains the data of Tremaine et al. (2011). The local meteoric water line (LMWL) equation determined for the northern part of the Carpathian Basin ($\delta^2\text{H} = 7.6 \cdot \delta^{18}\text{O} + 6.0$; Czuppon et al., 2018) was selected. This equation is very close to that of southern Hungary ($\delta^2\text{H} = 7.8 \cdot \delta^{18}\text{O} + 6.1$; Demény et al., 2021b, based on the 2004–2017 data of Fórizs et al., 2020), so the uncertainty of LMWL determination can be considered negligible. The formation temperatures obtained by this procedure are shown in Figure 8 as the $\delta^{18}\text{O}_{\text{cc}}$ -based dataset.

Another approach for paleotemperature calculations is based on the temperature-dependence of the hydrogen isotope compositions of precipitation water, for which the $\delta^2\text{H}$ -T gradient must be known (Demény et al., 2021b). The local gradient is 5‰/°C (Demény et al., 2021b). The $\delta^2\text{H}$ shift from the recent drip water composition (−71‰; Czuppon et al., 2022a), together with the $\delta^2\text{H}$ -T gradient, yields the temperature shift from the recent condition (8.8°C; Czuppon et al., 2022a), thus providing past temperatures. The $\delta^2\text{H}$ -based formation temperatures are also shown in Figure 8. The $\delta^2\text{H}$ -based procedure yielded generally reasonable temperatures between 7.8–9.7°C, except for three values ca. 8.5 ka. In contrast, the $\delta^{18}\text{O}_{\text{cc}}$ -based temperatures are too low (ca. 8.5 ka) and unrealistically high (8.25–8.1 ka). This may indicate diagenetic alteration in the $\delta^{18}\text{O}_{\text{cc}}$ values. However, without evidence of mineralogical change (e.g., aragonite to calcite transformation), strong recrystallization (e.g., appearance of mosaic fabric instead of columnar calcite), deposition of secondary carbonate (e.g., veins, pore fillings), or a diagenesis-sensitive porous texture, significant diagenetic alteration is not expected in a dense and compact calcite formation such as the V-03 stalagmite. Other causes of these results must be considered.

Seasonal signals in the inclusion-based stable isotope data

One possibility for the explanation of different calculated temperature records is the difference of seasonal signals in the $\delta^2\text{H}$ and $\delta^{18}\text{O}_{\text{cc}}$ records. The winter and summer laminae may have formed under different conditions, resulting in a difference in the efficiency of inclusion-water entrapment and a seasonal bias in the $\delta^2\text{H}$ values. To investigate this possibility, high-resolution $\delta^{13}\text{C}$ and $\delta^{18}\text{O}_{\text{cc}}$ analyses were conducted on the 8.25–8.1 ka section (Supplementary Fig. 4).

Two subsections (8.143–8.145 ka and 8.175–8.179 ka) yielded data at a resolution of 0.3 year, which may record winter and summer signals separately. The $\delta^{18}\text{O}$ fluctuations in these subsections are 0.3–0.5‰. Considering mixing during sampling, we can safely estimate that the difference in winter and summer $\delta^{18}\text{O}_{\text{cc}}$ values is ~0.5–1‰. This shift in the $\delta^{18}\text{O}_{\text{cc}}$ values would change the calculated temperatures by 2.2–4.5°C, bringing the $\delta^{18}\text{O}_{\text{cc}}$ -based temperature record close to the $\delta^2\text{H}$ -based one. This suggests that the low temperatures around 8.5 ka are due to winter-biased compositions, whereas the high temperatures between 8.25–8.1 ka are due to summer-biased values. This hypothesis may also explain the low $\delta^2\text{H}$ peak at ca. 8.5 ka assuming an elevated amount of winter precipitation, as well as the absence of a strong negative $\delta^2\text{H}$ peak at 8.2 ka, assuming increased summer precipitation and inclusion formation. High-resolution sampling was performed on half a stalagmite, and thin sections were produced from another half, precluding direct comparison with microscopic textures. Thus, the seasonality effect remains speculative. These considerations indicate that seasonal bias in inclusion formation is a potential explanation for the unrealistic formation temperatures calculated. These assumptions would also mean that, although the $\delta^{18}\text{O}_{\text{in}}$ values are diagenetically altered, the buffering capacity of the stalagmite calcite may help to preserve the $\delta^{18}\text{O}_{\text{cc}}$ values and that biased formation-temperature data may not necessarily mean diagenetic alteration occurred.

The change of hydrological conditions around 8.5 ka is further suggested by the growth axis drift (assumed on the basis of

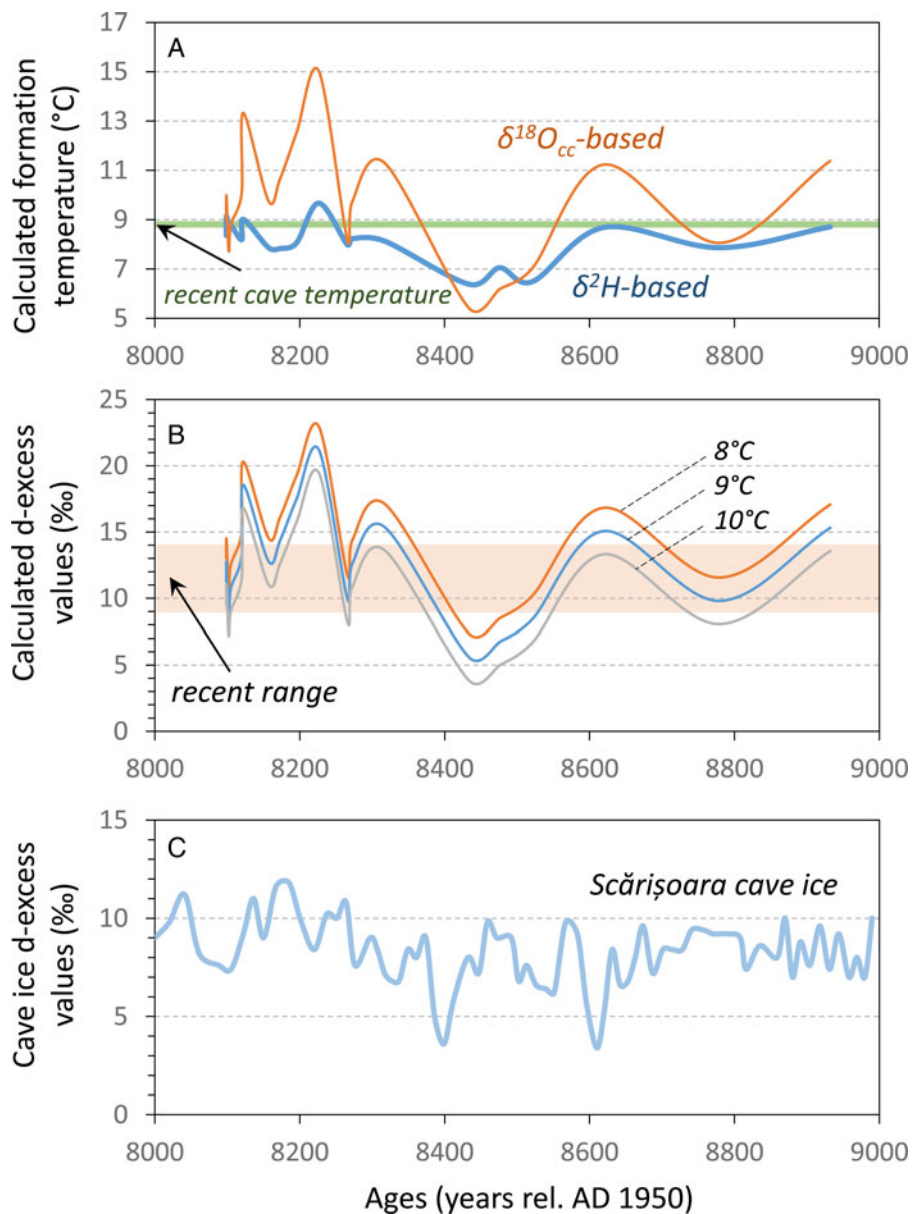


Figure 8. (A) Calculated temperatures (in °C) using the $\delta^{18}\text{O}_{\text{cc}}$ -based and the $\delta^2\text{H}$ -based methods (Demény et al., 2021b). (B) Calculated d-excess values for the V-03 stalagmite using formation temperatures of 8°C, 9°C, and 10°C. (C) Reported d-excess values for the Scărișoara Cave ice (Perșoiu et al., 2017).

inclusion trail shifts, Fig. 3) that, among other reasons, physical movement of the stalagmite or blockage of the drip water outflow, may indicate a change in drip-water flow from the feeding stalactite. However, the $\delta^2\text{H}$ variations are not associated with systematic changes in the humidity-proxy $\delta^{13}\text{C}$ and Sr records (Fig. 5), suggesting that precipitation variations do not indicate an annual decrease or increase, but rather a seasonal signal (i.e., an elevated amount of winter precipitation around 8.5 ka).

8.5 ka climate change event or local anomaly?

As we have shown, the V-03 stalagmite demonstrates a strongly negative $\delta^2\text{H}$ peak at 8.5 ± 0.1 ka, which is associated with a less-pronounced $\delta^{18}\text{O}_{\text{cc}}$ peak at 8.53 ka (Fig. 6). It is tempting to associate these isotope changes with the Laurentide Ice Sheet collapse and consequent freshwater discharge to the North Atlantic Ocean at 8420 ± 80 years (Tegzes et al., 2014), which may have induced climate change processes on the

European continent. These climate change effects may be indicated by the productivity and therefore the temperature and hydroclimate indicator TOC% of chlorines in the annually resolved record of Eifel maar lakes (Sirocko et al., 2021), the record of which shows a sharp rise at 8.52 ± 0.12 ka. Stable hydrogen isotope data that may be directly compared with the V-03 $\delta^2\text{H}$ record are scarce. Fluid inclusion data are available for speleothems from the Père Noël Cave (Belgium; Allan et al., 2018) and the Milandre Cave (Switzerland; Affolter et al., 2019), while cave ice data are available from the Scărișoara Cave (Perșoiu et al., 2017) (Fig. 6). Although the $\delta^2\text{H}$ change is minor in the Milandre record, it shows a broad negative peak between 8.75 ± 0.02 ka and 7.9 ± 0.04 ka, with a $\delta^2\text{H}$ change of -7‰ (Affolter et al., 2019). The Père Noël Cave record contains a sudden $\delta^2\text{H}$ shift from about -24‰ to -39‰ at 8.6 ka, and a slow increase to -33‰ at 7.9 ka (with an average error of ± 0.04 ka for the 7.9–8.6 ka section). The Scărișoara record has distinct negative $\delta^2\text{H}$ peaks at ca. 8.6 ka,

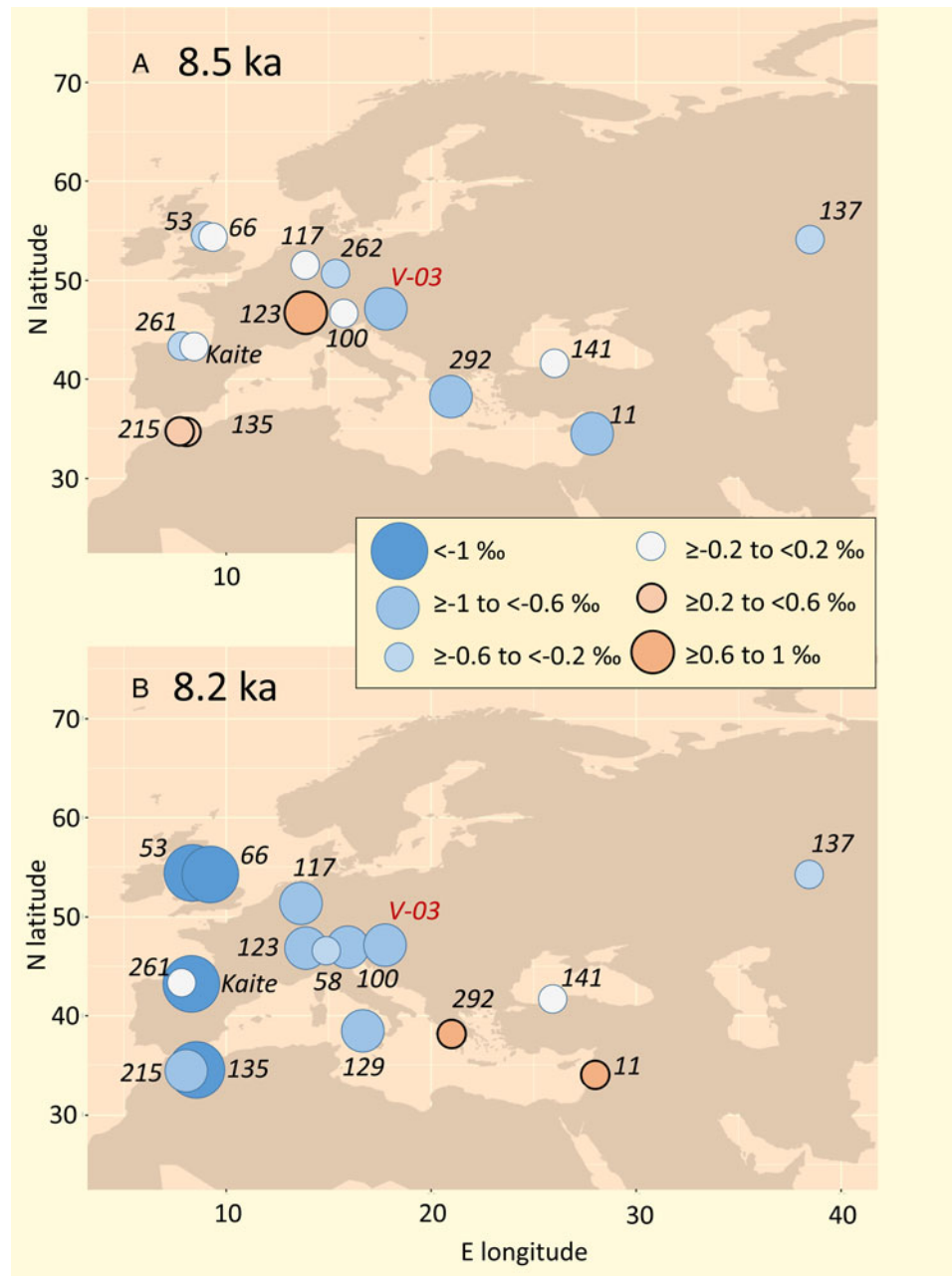


Figure 9. $\delta^{18}\text{O}_{\text{cc}}$ changes (in ‰) at (A) 8.5 ka and (B) 8.2 ka relative to the preceding 100 years of data in the individual records. The records used for the maps (shown in Supplementary Fig. 5) were gathered from the SISAL database (Atsawawaranunt *et al.*, 2018), excepting the Kaite cave record (Dominguez-Villar *et al.*, 2017) and the Vacska-03 record (this study). The numbers before cave names are SISAL entity codes. (11) Cheng *et al.* (2015). (53) and (66): Daley *et al.* (2013). (58): Fohlmeister *et al.* (2013). (100): Boch *et al.* (2009). (117): Fohlmeister *et al.* (2012). (123): Luetscher *et al.* (2011). (129): Frisia *et al.* (2006). (135) and (215): Ait Brahim *et al.* (2019). (137): Baker *et al.* (2017). (141): Fleitmann *et al.* (2009). (215): Ait Brahim *et al.* (2019). (261): Rossi *et al.* (2018) and Kilhavn *et al.* (2022). (262): Breitenbach *et al.* (2019). (292): Peckover *et al.* (2019).

8.4 ka, and 8.25 ka (Fig. 6) (with an average error of ± 0.34 ka for the 8.2–8.6 ka period).

To investigate if this presumed 8.5 ka climate change event appears in European speleothem records, the $\delta^{18}\text{O}_{\text{cc}}$ data of the SISAL database (Atsawawaranunt *et al.*, 2018) were gathered, and the relative $\delta^{18}\text{O}_{\text{cc}}$ changes at 8.5 ka were plotted on a map (Fig. 9A). The distribution of the isotope shifts does not reveal a systematic pattern, apart from the fact that similar $\delta^{18}\text{O}$ changes occur in the Vacska, Limnon (Greece), and Jeita (Lebanon) caves during the 8.6–8.4 ka period. This areal distribution suggests that the “8.5 ka event” (Demény *et al.*, 2022) is only a local or regional

phenomenon that may be indirectly related to the North Atlantic freshwater discharge but is a short-term climate anomaly.

Temperature and precipitation changes during the 8.2 ka event

The $\delta^{18}\text{O}_{\text{cc}}$ values depend on both formation temperature and water composition. Surface temperatures are generally positively correlated with $\delta^{18}\text{O}_{\text{w}}$ values (about $+0.6 \text{ ‰}/^\circ\text{C}$; Demény *et al.*, 2021b), while formation temperature increase causes a $-0.23 \text{ ‰}/^\circ\text{C}$ change in speleothems (Tremaine *et al.*, 2011). As a result, the

net $\delta^{18}\text{O}_{\text{cc}}$ change with temperature is $\sim 0.37\text{‰}/\text{°C}$. The average $\delta^{18}\text{O}_{\text{cc}}$ value for the 8.25–8.5 ka period is $-9.0 \pm 0.4\text{‰}$, and the lowest $\delta^{18}\text{O}_{\text{cc}}$ value at 8.18 ka is -9.8‰ . The -0.8‰ shift corresponds to a 2.1°C cooling, provided that the recent $\delta^{18}\text{O}$ -temperature relationship is valid. It should be noted, however, that this temperature change is an estimated maximum, because it was calculated using the lowest $\delta^{18}\text{O}_{\text{cc}}$ value. Within the negative $\delta^{18}\text{O}_{\text{cc}}$ peak, the $\delta^{13}\text{C}$ values first increase to -8.6‰ at 8.23 ka and then decrease to -10.2‰ at 8.18 ka when the $\delta^{18}\text{O}_{\text{cc}}$ record reaches its minimum. This observation suggests that the first part of the 8.2 ka event is associated with strong fluctuations in soil activity. The Sr contents are low (Fig. 5), suggesting either dilution, and therefore a higher amount of precipitation, or decreased weathering in the soil zone. The $\delta^2\text{H}$ values are not shifted in a negative direction, indicating an elevated relative contribution of summer precipitation. In summary, the first part of the 8.2 ka event period is characterized by general cooling, a relatively elevated precipitation amount in the summer, and fluctuating soil activity, which are unfavorable climate conditions for vegetation. The strong $\delta^{13}\text{C}$ fluctuation and the decreased soil-zone weathering indicate changing dry/wet conditions during the cooling period. In the 40–70 mm dft (ca. 8.38–8.1 ka) section of the V-03 stalagmite, the U-Th age model would fit a ^{14}C -based age model with $>8\%$ dcp, whereas the other parts of the U-Th-based StalAge model curve would fall between the 5% and 8% dcp ^{14}C model curves (Fig. 4). The elevated dead carbon contribution would be consistent with positive $\delta^{13}\text{C}$ shifts and generally lower Sr concentrations in the 40–70 mm dft section in case of soil activity decrease (i.e., less biogenic carbon contribution) and reduced weathering in the soil zone due to cooling and/or drying, but with transient humid conditions (water-filled karstic system precluding exchange with atmospheric CO_2 ; Noronha et al., 2014), again suggesting fluctuating precipitation amounts.

Just before the hiatus at 48.0 mm (corresponding to a model age of 8.15 ka), the $\delta^{13}\text{C}$ and $\delta^{18}\text{O}_{\text{cc}}$ values rise markedly, indicating dry conditions, before finally resulting in a growth stop. This short period may be followed by a sudden increase in precipitation amount, likely with a decrease in pH levels (i.e., dissolution surface on the stalagmite) due to elevated biogenic CO_2 dissolution. The increase in precipitation amount, as well as the more favorable soil conditions are indicated by the generally low $\delta^{13}\text{C}$ values after 8.15 ka and the slightly elevated Sr concentrations, the latter related to enhanced weathering in the soil zone.

Similar temperature/precipitation changes have been inferred in lake deposits (Pál et al., 2016), as well as in speleothems and alluvial fan sediments (Peckover et al., 2019) in Southeast Europe. Pál et al. (2016) investigated seasonal temperature and precipitation amount changes using pollen concentrations, biogenic silica percentage determinations, and diatom distributions in lake sediments in the Retezat Mountains (Southern Romania). Microcharcoal pieces, Poaceae, *Corylus*, *Quercus*, *Ulmus*, and *Picea* pollen show peaks at 8.3–8.25 ka (with an error of about ± 0.1 ka), followed by a sharp peak of *Carpinus betulus* and planktonic diatom taxa at 8.15 ka. These pieces of information would collectively suggest that the 8.2 ka cooling was associated with alternation of dry/warm summers, and then precipitation amount and winter temperature increased (Pál et al., 2016). Similar temperature and precipitation changes are inferred from the combined analyses of a speleothem (growth rate, $\delta^{13}\text{C}$, $\delta^{18}\text{O}$, and trace element concentrations) and alluvial fan sediments in Greece by Peckover et al. (2019). The combined

evaluation of these proxy records led Peckover et al. (2019) to conclude that the 8.2 ka event was cold and dry, with “flashier” summer rainfall, and a humid phase after 8.1 ka. These precipitation and temperature changes are in agreement with the coupled $\delta^2\text{H}$ - $\delta^{13}\text{C}$ - $\delta^{18}\text{O}_{\text{cc}}$ -Sr changes in the V-03 stalagmite results reported in this paper, as well as the growth stop and short-term dissolution at 8.15 ka.

Moisture transport changes reflected by d-excess data

Moisture transport trajectories may be inferred from d-excess values ($d = \delta^2\text{H} - 8 \cdot \delta^{18}\text{O}$) because moisture originating from the Atlantic Ocean has generally lower d-excess values than moisture that comes from the Mediterranean Sea (Gat, 1980; Gat and Carmi, 1987). The $\delta^{18}\text{O}_{\text{w}}$ data can be calculated from the $\delta^{18}\text{O}_{\text{cc}}$ values, the estimated formation temperatures, and the calcite-water oxygen isotope fractionation in Johnston et al. (2013), after which the d-excess values may be computed from the measured $\delta^2\text{H}$ and calculated $\delta^{18}\text{O}_{\text{w}}$ values. Formation temperatures were estimated to be 8–10°C (recent cave temperature is 8.8°C). The obtained d-excess values range from 3.8–23.0‰, with remarkably low and high values around 8.5 ka and 8.2 ka respectively (Fig. 8B). Assuming the same seasonal $\delta^{18}\text{O}_{\text{cc}}$ bias as discussed previously, the range would become 6.7–15.3‰, which is similar to the range of 9–14‰ obtained from recent precipitation monitoring data (Czuppon et al., 2018). These calculations indicate that the d-excess values would fit the observed range when using the hypothetical summer precipitation bias.

The uncorrected d-excess values seem unrealistic, so the $\delta^{18}\text{O}_{\text{cc}}$ correction must be assumed to arrive at a reasonable range. Nevertheless, the calculations may indicate that the 8.6–8.4 ka period is dominated by low d-excess values, whereas the 8.3–8.1 ka period is characterized by elevated d-excess values. The d-excess record of the Scărișoara cave ice (Perșoiu et al., 2017) also indicates elevated values at 8.2 ka (Fig. 8C), which were attributed to an increased contribution of Mediterranean moisture. It is important to note that low d-excess peaks appear at ca. 8.6 ka and 8.4 ka in the Scărișoara record, which may be correlated with the low d-excess values of the V-03 stalagmite in this study.

Elevated d-excess values and the inferred Mediterranean moisture contribution are indirect indicators of moisture-transport changes. Moisture trajectory shifts and varying degrees of Mediterranean moisture contribution have been inferred for the Katerloch Cave (Austrian Alps), where speleothem records spanning the 8.2 ka event have been gathered (Boch et al., 2009). Parker and Harrison (2022) assumed that global transfer of the low $\delta^{18}\text{O}$ signal associated with the 8.2 ka event was due to the southward shift of the Intertropical Convergence Zone (ITCZ), which affected climate conditions all over the world. The southward movement of the ITCZ would also have induced a north-south displacement of moisture transport from the northern part of the North Atlantic Ocean to the southern regions. Although model calculations indicate a weakening of the low $\delta^{18}\text{O}$ signal below 40°N latitude (Wiersma et al., 2011), the speleothem $\delta^{18}\text{O}$ records show negative $\delta^{18}\text{O}$ shifts, even in Morocco, until the negative $\delta^{18}\text{O}$ signal increasingly diminishes towards the East (Fig. 9B). The drawbacks in model calculations also appear in the duration of the 8.2 ka event. Wiersma et al. (2011) estimated it to last around 60 years, whereas the speleothem records generally suggest a longer duration of about 160 years.

Other than the southward shift of moisture transport and increased Mediterranean contribution to the precipitation in East-Central Europe (Perşoiu *et al.*, 2017, and this study), we also suggest that the amount of precipitation changed seasonally, with a relatively increased summer contribution. This is in accordance with the positive $\delta^{18}\text{O}$ changes in the eastern part of the Mediterranean, where the oxygen isotope composition of rainwater, and therefore of speleothems, is primarily governed by precipitation amount, as shown by the compilation of regional speleothem records in Kern *et al.* (2019).

Conclusion

A stalagmite was collected in northern Hungary from a carefully selected site (Vacska Cave), where ventilation was negligible compared to other parts of the cave system, and that was monitored for two years for physical cave parameters and drip water compositions. Fourteen U-Th age dates suggest that the stalagmite covers the period of 10.6–8.0 ka (relative to AD 1950). In this study, the 8–9 ka section was thoroughly investigated using petrographic observations, AMS ^{14}C measurements, XRF-based Sr concentration measurements, and stable H, C, and O isotope analyses of stalagmite calcite and inclusion-hosted water. A $\delta^{18}\text{O}_{\text{cc}}$ peak with an approximately -0.8‰ shift between 8.25–8.1 ka was observed, which may be related to the 8.2 ka event. Additionally, negative $\delta^{18}\text{O}_{\text{cc}}$ and $\delta^2\text{H}$ peaks appear at ca. 8.5 ka. Using a compilation of European and eastern Mediterranean speleothem data from the SISAL database (Atsawaranunt *et al.*, 2018), the “8.5 ka event” was actually determined to be a local or regional climate anomaly that may have had indirect connections with North Atlantic freshwater discharge.

Stable oxygen isotope compositions of inclusion-hosted water were evaluated for a paleoclimate interpretation, but their correlation with the carbonate crystallinity indicator FWHM of the main X-ray diffraction peak instead indicated that diagenetic alteration occurred, which superseded the primary climate-related information. The petrographic and geochemical observations for the 8.25–8.1 ka period revealed a series of temperature and precipitation changes during the 8.2 ka event. After the event's peak conditions (strong cooling and drying), the local climate became humid and warm, with a sudden and sharp change at 8.15 ka. The 8.2 ka event peak was associated with relatively increased d-excess values, indicating increased Mediterranean moisture contribution. This change in the origin of the moisture is in agreement with the southward displacement of heat and moisture-transport trajectories during the 8.2 ka event, as inferred by previous studies and shown by the regional distribution of 8.2 ka $\delta^{18}\text{O}$ peaks of speleothem records gathered from the SISAL database.

Supplementary Material. The supplementary material for this article can be found at <https://doi.org/10.1017/qua.2023.33>

Acknowledgments. The LA-ICP-MS analyses were performed by Dr. Sébastien Pilet at the University of Lausanne, who we gratefully thank. Ágnes Berentés and Richárd Kovács provided essential help in cave research. The authors are indebted to Ariana Gugora for polishing the English of the manuscript. Constructive reviews and helpful comments of two anonymous reviewers, and the editorial handling by Andrea Columbu are gratefully thanked. The study was financed by the Eötvös Loránd Research Network (SA-41/2021). The MC-ICP-MS and MICADAS facilities of the Institute for Nuclear Research, Debrecen, were supported by the National Research, Development and Innovation Office (GINOP-2.3.2-15-2016-00009). We are

also grateful for the support and permission (2148-8/2019) of the Duna-Ipoly National Park Directorate.

References

- Affolter, S., Häuselmann, A., Fleitmann, D., Edwards, R. L., Cheng, H., Leuenberger, M., 2019. Central Europe temperature constrained by speleothem fluid inclusion water isotopes over the past 14,000 years. *Science Advances* 5, eaav3809. <https://doi.org/10.1126/sciadv.aav3809>.
- Ait Brahim, Y., Wassenburg, J.A., Sha, L., Cruz, F.W., Deininger, M., Sifeddine, A., Bouchaou, L., Spötl, C., Edwards, R.L., Cheng, H., 2019. North Atlantic ice-rafting, ocean and atmospheric circulation during the Holocene: insights from Western Mediterranean speleothems. *Geophysical Research Letters* 46, 7614–7623.
- Allan, M., Fagel, N., van der Lubbe, H.J.L., Vonhof, H.B., Cheng, H., Edwards, R.L., Verheyden, S., 2018. High-resolution reconstruction of 8.2 ka event documented in Père Noël cave, southern Belgium. *Journal of Quaternary Science* 33, 840–852.
- Alley, R.B., Mayewski, P.A., Sowers, T., Stuiver, M., Taylor, K.C., Clark, P.U., 1997. Holocene climatic instability: a prominent, widespread event 8200 yr ago. *Geology* 25, 483–486.
- Atsawaranunt, K., Comas-Bru, L., Amirnezhad Mozhdehi, S., Deininger, M., Harrison, S. P., Baker, A., Boyd, M., *et al.*, 2018. The SISAL database: a global resource to document oxygen and carbon isotope records from speleothems. *Earth System Science Data* 10, 1687–1713.
- Baker, J.L., Lachniet, M.S., Chervyatsova, O., Asmerom, Y., Polyak, V.J., 2017. Holocene warming in western continental Eurasia driven by glacial retreat and greenhouse forcing. *Nature Geoscience* 10, 430–435.
- Barber, D.C., Dyke, A., Hillaire-Marcel, C., Jennings, A.E., Andrews, J.T., Kerwin, M.W., Bilodeau, G., *et al.*, 1999. Forcing of the cold event of 8,200 years ago by catastrophic drainage of Laurentide lakes. *Nature* 400, 344–348.
- Benson, A., Hoffmann, D.L., Daura, J., Sanz, M., Rodrigues, F., Souto, P., Zilhão, J., 2021. A speleothem record from Portugal reveals phases of increased winter precipitation in western Iberia during the Holocene. *The Holocene* 31, 1339–1350.
- Boch, R., Spötl, C., Kramers, J., 2009. High-resolution isotope records of early Holocene rapid climate change from two coeval stalagmites of Katerloch Cave, Austria. *Quaternary Science Reviews* 28, 2527–2538.
- Borsato, A., Johnston, V.E., Frisia, S., Miorandi, R., Corradini, F., 2016. Temperature and altitudinal influence on karst dripwater chemistry: implications for regional-scale palaeoclimate reconstructions from speleothems. *Geochimica et Cosmochimica Acta* 177, 275–297.
- Breitenbach, S.F.M., Plessen, B., Waltgenbach, S., Tjallingii, R., Leonhardt, J., Jochum, K.P., Meyer, H., Goswami, B., Marwan, N., Scholz, D., 2019. Holocene interaction of maritime and continental climate in Central Europe: new speleothem evidence from central Germany. *Global and Planetary Change* 176, 144–161.
- Bronk Ramsey, C., 2001. Development of the radiocarbon calibration program OxCal. *Radiocarbon* 43, 355–363.
- Bronk Ramsey, C., 2008. Deposition models for chronological records. *Quaternary Science Reviews* 27, 42–60.
- Brouard, E., Roy, M., Godbout, P.-M., Veillette, J.J., 2021. A framework for the timing of the final meltwater outbursts from glacial Lake Agassiz-Ojibway. *Quaternary Science Reviews* 274, 107269. <https://doi.org/10.1016/j.quascirev.2021.107269>.
- Cheng, H., Fleitmann, D., Edwards, R.L., Wang, X., Cruz, F.W., Auler, A.S., Mangini, A., *et al.*, 2009. Timing and structure of the 8.2 kyr B.P. event inferred from $\delta^{18}\text{O}$ records of stalagmites from China, Oman, and Brazil. *Geology* 37, 1007–1010.
- Cheng, H., Sinha, A., Verheyden, S., Nader, F.H., Li, X.L., Zhang, P.Z., Yin, J.J., *et al.*, 2015. The climate variability in northern Levant over the past 20,000 years. *Geophysical Research Letters* 42, 8641–8650.
- Czuppon, Gy., Demény, A., Leél-Össy, Sz., Óvari, M., Molnár, M., Stieber, J., Kiss, K., Kármán, K., Surányi, G., Haszpra, L., 2018. Cave monitoring in the Béke and Baradla caves (northeastern Hungary): implications for the conditions for the formation cave carbonates. *International Journal of Speleology* 47, 13–28.

- Czuppon, Gy., Demény, A., Leél-Óssy, Sz., Stieber, J., Óvári, M., Dobosy, P., Berentés, Á., Kovács, R., 2022a. Cave monitoring in Hungary: an overview. *Central European Geology* **65**, 26–39.
- Czuppon, Gy., Demény, A., Leél-Óssy, Sz., Stieber, J., Óvári, M., Dobosy, P., Berentés, Á., Kovács, R., 2022b. Monitoring and geochemical investigations of caves in Hungary: Implications for climatological, hydrological, and speleothem formation processes. In: Veress, M., Leél-Óssy, Sz. (Eds.), *Cave and Karst Systems of Hungary*. Springer Nature, Cham, Switzerland, pp. 465–486.
- Daley, T.J., Thomas, E.R., Holmes, J.A., Street-Perrott, F.A., Chapman, M.R., Tindall, J.C., Valdes, P.J., et al., 2013. The 8200yr cold event in stable isotope records from the North Atlantic region. *Global and Planetary Change* **79**, 288–302.
- Deák, I., Leél-Óssy, Sz., Kövér, Sz., Surányi, G., 2007. A Csévi-szirtek barlangjai. [Caves of the Csévi-Cliffs]. *Karszt és Barlang [Karst and Cave]* **2007**, 17–36. [in Hungarian]
- Demény, A., Berentés, Á., Czuppon, Gy., Kovács, R., Leél-Óssy, Sz., Surányi, G., 2021c. Nyitni vagy nem nyitni? –Pilis barlangok szellőzöttsége a geokémiai adatok tükrében. [To open or not to open? Ventilation in the Pilis caves in the light of geochemical data]. *Földrajzi Közlemények* **145**, 224–231.
- Demény, A., Czuppon, Gy., Kern, Z., Leél-Óssy, Sz., Németh, A., Szabó, M., Tóth, M., et al., 2016. Recrystallization-induced oxygen isotope changes in inclusion-hosted water of speleothems—paleoclimatological implications. *Quaternary International* **415**, 25–32.
- Demény, A., Kern, Z., Czuppon, Gy., Németh, A., Leél-Óssy, Sz., Siklós, Z., Lin, K., et al., 2017. Stable isotope compositions of speleothems from the last interglacial—spatial patterns of climate fluctuations in Europe. *Quaternary Science Reviews* **161**, 68–80.
- Demény, A., Kern, Z., Czuppon, Gy., Németh, A., Schöll-Barna, G., Siklós, Z., Leél-Óssy, Sz., et al., 2019a. Middle Bronze Age humidity and temperature variations, and societal changes in East-Central Europe. *Quaternary International* **504**, 80–95.
- Demény, A., Kern, Z., Hatvani, I.G., Torma, Cs., Topál, D., Frisia, S., Leél-Óssy, Sz., Czuppon, Gy., Surányi, G., 2021a. Holocene hydrological changes in Europe and the role of the North Atlantic ocean circulation from a speleothem perspective. *Quaternary International* **571**, 1–10.
- Demény, A., Kern, Z., Németh, A., Frisia, S., Hatvani, I.G., Czuppon, Gy., Leél-Óssy, Sz., et al., 2019b. North Atlantic influences on climate conditions in East-Central Europe in the Late Holocene reflected by flowstone compositions. *Quaternary International* **512**, 99–112.
- Demény, A., Rinyu, L., Kern, Z., Hatvani, I.G., Czuppon, Gy., Surányi, G., Leél-Óssy, Sz., Shen, Ch.-Ch., Koltai, G., 2021b. Paleotemperature reconstructions using speleothem fluid inclusion analyses from Hungary. *Chemical Geology* **563**, 120051. <https://doi.org/10.1016/j.chemgeo.2020.120051>.
- Demény, A., Topál, D., Surányi, G., Czuppon, Gy., Berentés, Á., Molnár, M., Leél-Óssy, Sz., Kovács, R., 2022. *Climate change event at 8.5 ka detected from Oman to the Carpathian Basin: teleconnections with the Indian ocean. Climate Change: The Karst Record IX (KR9)*, University of Innsbruck, Austria, Abstracts, p. 101.
- Domínguez-Villar, D., Wang, X., Krklec, K., Cheng, H., Edwards, R.L., 2017. The control of the tropical North Atlantic on Holocene millennial climate oscillations. *Geology* **45**, 303–306.
- Dreybrodt, W., Fohlmeister, J., 2022. The impact of outgassing of CO₂ and prior calcium precipitation to the isotope composition of calcite precipitated on stalagmites. Implications for reconstructing climate information from proxies. *Chemical Geology* **589**, 120676. <https://doi.org/10.1016/j.chemgeo.2021.120676>.
- Fairchild, I.J., Baker, A., 2012. *Speleothem Science*. Wiley-Blackwell, Chichester, UK, 450 pp.
- Fairchild, I.J., Baker, A., Borsato, A., Frisia, S., Hinton, R.W., McDermott, F., Tooth, A.F., 2001. Annual to sub-annual resolution of multiple trace-element trends in speleothems. *Journal of the Geological Society* **158**, 831–841.
- Fleitmann, D., Burns, S.J., Mangini, A., Mudelsee, M., Kramers, J., Villa, I., Neff, U., et al., 2007. Holocene ITCZ and Indian monsoon dynamics recorded in stalagmites from Oman and Yemen (Socotra). *Quaternary Science Reviews* **26**, 170–188.
- Fleitmann, D., Cheng, H., Badertscher, S., Edwards, R. L., Mudelsee, M., Göktürk, O. M., Fankhauser, A., et al., 2009. Timing and climatic impact of Greenland interstadials recorded in stalagmites from northern Turkey. *Geophysical Research Letters* **36**, L19707. <https://doi.org/10.1029/2009GL040050>.
- Fohlmeister, J., Schröder-Ritzrau, A., Scholz, D., Spötl, C., Riechelmann, D. F. C., Mudelsee, M., Wackerbarth, A., et al., 2012. Bunker Cave stalagmites: an archive for central European Holocene climate variability. *Climate of the Past* **8**, 1751–1764.
- Fohlmeister, J., Vollweiler, N., Spötl, C., Mangini, A., 2013. COMNISPA II: update of a mid-European isotope climate record, 11 ka to present. *The Holocene* **23**, 749–754.
- Fórizs, I., Kern, Z., Csicsák, J., Csurgó, G., Földing, G., Máthé, Z., Ország, J., Szreda, G., Vendégh, R., 2020. Monthly data of stable isotopic composition ($\delta^{18}\text{O}$, $\delta^2\text{H}$) and tritium activity in precipitation from 2004 to 2017 in the Mecsek Hills, Hungary. *Data in Brief* **32**, 106206. <https://doi.org/10.1016/j.dib.2020.106206>.
- Frisia, S., Borsato, A., Mangini, A., Spötl, C., Madonia, G., Sauro, U., 2006. Holocene Climate variability in Sicily from a discontinuous stalagmite record and the Mesolithic to Neolithic transition. *Quaternary Research* **66**, 388–400. <https://doi.org/10.1016/j.yqres.2006.05.003>.
- Gat, J.R., 1980. The isotopes of hydrogen and oxygen in precipitation. In: Fritz, P., Fontes, G. (Eds.), *Handbook of Environmental Isotope Geochemistry*. Elsevier, Amsterdam, pp. 21–47.
- Gat, J.R., Carmi, I., 1987. Effect of climate changes on the precipitation patterns and isotopic composition of water in a climate transition zone: case of the Eastern Mediterranean sea area. In: Solomon, S.I., Beran, M., Hogg, W. (Eds.), *The Influence of Climate Change and Climatic Variability on the Hydrologic Regime and Water Resources*. Proceedings, of the Vancouver Symposium, IAHS Publication No. 168, pp. 513–523.
- Gkinis, V., Vinther, B.M., Popp, T.J., Quistgaard, T., Faber, A.K., Holme, C.T., Jensen, C.M., et al., 2021. A 120,000-year long climate record from a NW-Greenland deep ice core at ultra-high resolution. *Scientific Data* **8**, 141. <https://doi.org/10.1038/s41597-021-00916-9>.
- Haas, J. (Ed.), 2001. *Geology of Hungary*. Eötvös Kiadó [Eötvös University Press], Budapest.
- Huang, Y., Fairchild, I.J., 2001. Partitioning of Sr²⁺ and Mg²⁺ into calcite under karst-analogue experimental conditions. *Geochimica et Cosmochimica Acta* **65**, 47–62.
- Hua, Q., Barbetti, M., Rakowski, A.Z., 2013. Atmospheric radiocarbon for the period 1950–2010. *Radiocarbon* **55**, 2059–2072.
- Johnston, V.E., Borsato, A., Spötl, C., Frisia, S., Miorandi, R., 2013. Stable isotopes in caves over altitudinal gradients: fractionation behaviour and inferences for speleothem sensitivity to climate change. *Climate of the Past* **9**, 99–118.
- Kern, Z., Demény, A., Persoiu, A., Hatvani, I.G., 2019. Speleothem records from the eastern part of Europe and Turkey—discussion on stable oxygen and carbon isotopes. *Quaternary* **2**, 31. <https://doi.org/10.3390/quat2030031>.
- Kilhván, H., Couchoud, I., Drysdale, R.N., Rossi, C., Hellstrom, J., Arnaud, F., Wong, H., 2022. The 8.2 ka event in northern Spain: timing, structure and climatic impact from a multi-proxy speleothem record. *Climate of the Past* **18**, 2321–2344.
- Lachniet, M.S., 2009. Climatic and environmental controls on speleothem oxygen-isotope values. *Quaternary Science Reviews* **28**, 412–432.
- Landis, G.P., 1983. Harding Iceland Spar: a new $\delta^{18}\text{O}$ – $\delta^{13}\text{C}$ carbonate standard for hydrothermal minerals. *Isotope Geoscience* **1**, 91–94.
- Luetscher, M., Hoffmann, D.L., Frisia, S., Spötl, C., 2011. Holocene glacier history from alpine speleothems, Milchbach Cave, Switzerland. *Earth and Planetary Science Letters* **302**, 95–106.
- Major, I., Haszpra, L., Rinyu, L., Futó, I., Bihari, Á., Hammer, S., Jull, A.J.T., Molnár, M., 2018. Temporal variation of atmospheric fossil and modern CO₂ excess at a Central European rural tower station between 2008 and 2014. *Radiocarbon* **60**, 1285–1299.
- McCrea, J.M., 1950. On the isotopic chemistry of carbonates and a paleotemperature scale. *The Journal of Chemical Physics* **18**, 849–857.
- Mickler, P.J., Banner, J.L., Stern, L., Asmerom, Y., Edwards, R.L., Ito, E., 2004. Stable isotope variations in modern tropical speleothems: evaluating applications to paleoenvironmental reconstructions. *Geochimica et Cosmochimica Acta* **68**, 4381–4393.

- Mickler, P.J., Stern, L.A., Banner, J.L., 2006. Large kinetic isotope effects in modern speleothems. *GSA Bulletin* **118**, 65–81.
- Molnár, M., Dezső, Z., Futó, I., Rinyu, L., Svingor, É., 2006. Measurement and interpretation of ^{14}C -contents of young karstic rocks. *Karst Development (Karszfajlódás)* **11**, 37–46. [in Hungarian]
- Molnár, M., Dezső, Z., Futó, I., Siklósy, Z., Jull, A.J.T., Koltai, G., 2016. Study of radiocarbon dynamics of Baradla Cave, Hungary. *Geophysical Research Abstracts* **18**, EGU2016-15278-1.
- Molnár, M., Janovics, R., Major, I., Orsovski, J., Gönczi, R., Veres, M., Leonard, A.G., *et al.*, 2013a. Status report of the new AMS ^{14}C sample preparation lab of the Hertelendi Laboratory of Environmental Studies, Debrecen, Hungary. *Radiocarbon* **55**, 665–676.
- Molnár, M., Rinyu, L., Veres, M., Seiler, M., Wacker, L., Synal, H.-A., 2013b. EnvironMICADAS: a mini ^{14}C AMS with enhanced gas ion source interface in the Hertelendi Laboratory of Environmental Studies (HEKAL), Hungary. *Radiocarbon* **55**, 338–344.
- Morrill, C., Anderson, D.M., Bauer, B.A., Buckner, R., Gille, E.P., Gross, W.S., Hartman, M., Shah, A., 2013. Proxy benchmarks for intercomparison of 8.2 ka simulations. *Climate of the Past* **9**, 423–432.
- Neff, U., Burns, S.J., Mangini, A., Mudelsee, M., Fleitmann, D., Matter, A., 2001. Strong coherence between solar variability and the monsoon in Oman between 9 and 6 kyr ago. *Nature* **411**, 290–293.
- Noronha, A.L., Johnson, K.R., Hu, C., Ruan, J., Southon, J.R., Ferguson, J.E., 2014. Assessing influences on speleothem dead carbon variability over the Holocene: implications for speleothem-based radiocarbon calibration. *Earth and Planetary Science Letters* **394**, 20–29.
- Pál, I., Magyari, E.K., Braun, M., Vincze, I., Pálffy, J., Molnár, M., Finsinger, W., Buczkó, K., 2016. Small-scale moisture availability increase during the 8.2 ka climatic event inferred from biotic proxy records in the South Carpathians (SE Romania). *The Holocene* **26**, 1382–1396.
- Parker, S.E., Harrison, S.P., 2022. The timing, duration and magnitude of the 8.2 ka event in global speleothem records. *Scientific Reports* **12**, 10542. <https://doi.org/10.1038/s41598-022-14684-y>.
- Peckover, E.N., Andrews, J.E., Leeder, M.R., Rowe, P.J., Marca, A., Sahy, D., Noble, S., Gawthorpe, R., 2019. Coupled stalagmite—alluvial fan response to the 8.2 ka event and Early Holocene palaeoclimate change in Greece. *Palaeogeography, Palaeoclimatology, Palaeoecology* **532**, 109252. <https://doi.org/10.1016/j.palaeo.2019.109252>.
- Perşoiu, A., Onac, B.P., Wynn, J.G., Blaauw, M., Ionita, M., Hansson, M., 2017. Holocene winter climate variability in Central and Eastern Europe. *Scientific Reports* **7**, 1196. <https://doi.org/10.1038/s41598-017-01397-w>.
- Prasad, S., Witt, A., Kienel, U., Dulski, P., Bauer, E., Yancheva, G., 2009. The 8.2 ka event: evidence for seasonal differences and the rate of climate change in western Europe. *Global and Planetary Change* **67**, 218–226.
- Railsback, L.B., Akers, P.D., Wang, L., Holdridge, G.A., Voarintsoa, Ny.R., 2013. Layer-bounding surfaces in stalagmites as keys to better paleoclimatological histories and chronologies. *International Journal of Speleology* **42**, 167–180.
- Reimer, P.J., Austin, W.E.N., Bard, E., Bayliss, A., Blackwell, P.G., Bronk Ramsey, C., Butzin, M., *et al.*, 2020. The IntCal20 Northern Hemisphere radiocarbon age calibration curve (0–55 cal k). *Radiocarbon* **62**, 725–757.
- Rinyu, L., Molnár, M., Major, I., Nagy, T., Veres, M., Kimák, Á., Wacker, L., Synal, H.-A., 2013. Optimization of sealed tube graphitization method for environmental C-14 Studies Using MICADAS. *Nuclear Instruments and Methods in Physics Research, Section B: Beam Interactions With Materials and Atoms* **294**, 270–275.
- Rohling, E.J., Pälike, H., 2005. Centennial-scale climate cooling with a sudden cold event around 8,200 years ago. *Nature* **434**, 975–979.
- Rossi, C., Bajo, P., Lozano, R. P., Hellstrom, J., 2018. Younger Dryas to Early Holocene paleoclimate in Cantabria (N Spain): constraints from speleothem Mg, annual fluorescence banding and stable isotope records. *Quaternary Science Reviews* **192**, 71–85.
- Scholz, D., Hoffmann, D.L., 2011. StalAge—an algorithm especially designed for construction of speleothem age models. *Quaternary Geochronology* **6**, 369–382.
- Seppä, H., Birks, H.J.B., Giesecke, T., Hammarlund, D., Alenius, T., Antonsson, K., Bjune, A.E., *et al.*, 2007. Spatial structure of the 8200 cal yr event in northern Europe. *Climate of the Past* **3**, 225–236.
- Sha, L., Ait Brahim, Y., Wassenburg, J.A., Yin, J., Peros, M., Cruz, F.W., Cai, Y., *et al.*, 2019. How far north did the African Monsoon fringe expand during the African Humid Period? Insights from Southwest Moroccan speleothems. *Geophysical Research Letters* **46**, 14093–14102.
- Shi, X., Lohmann, G., Sidorenko, D., Yang, H., 2020. Early-Holocene simulations using different forcings and resolutions in AWI-ESM. *The Holocene* **30**, 996–1015.
- Siklósy, Z., Demény, A., Vennemann, T.W., Pilet, S., Kramers, J., Leél-Össy, S., Bondár, M., Shen, C.-C., Hegner, E., 2009. Bronze Age volcanic event recorded in stalagmites by combined isotope and trace element studies. *Rapid Communication in Mass Spectrometry* **23**, 801–808.
- Sinclair, D.J., 2011. Two mathematical models of Mg and Sr partitioning into solution during incongruent calcite dissolution. Implications for dripwater and speleothem studies. *Chemical Geology* **283**, 119–133.
- Sirocko, F., Martínez-García, A., Mudelsee, M., Albert, J., Britzius, S., Christl, M., Diehl, D., *et al.*, 2021. Muted multidecadal climate variability in central Europe during cold stadial periods. *Nature Geoscience* **14**, 651–658.
- Steponaitis, E., Andrews, A., McGee, D., Quade, J., Hsieh, Y.T., Broecker, W.S., Shuman, B.N., Burns, S.J., Cheng, H., 2015. Mid-Holocene drying of the U.S. Great Basin recorded in Nevada speleothems. *Quaternary Science Reviews* **127**, 174–185.
- Tegzes, A.D., Jansen, E., Telford, R.J., 2014. The role of the northward-directed (sub)surface limb of the Atlantic Meridional Overturning Circulation during the 8.2 ka event. *Climate of the Past* **10**, 1887–1904.
- Thomas, E.R., Wolff, E.W., Mulvaney, R., Steffensen, J.P., Johnsen, S.J., Arrowsmith, C., White, J.W.C., Vaughn, B., Popp, T., 2007. The 8.2 ky event from Greenland ice cores. *Quaternary Science Reviews* **26**, 70–81.
- Tremaine, D.M., Froelich, P.N., Wang, Y., 2011. Speleothem calcite farmed in situ: modern calibration of $\delta^{18}\text{O}$ and $\delta^{13}\text{C}$ paleoclimate proxies in a continuously-monitored natural cave system. *Geochimica et Cosmochimica Acta* **75**, 4929–4950.
- Wiersma, A.P., Roche, D.M., Renssen, H., 2011. Fingerprinting the 8.2 ka event climate response in a coupled climate model. *Journal of Quaternary Science* **26**, 118–127.